



UNIVERSITÀ
DEGLI STUDI
FIRENZE

FLORE

Repository istituzionale dell'Università degli Studi di Firenze

Microfossil evidence for trophic changes during the Eocene-Oligocene transition in the South Atlantic (ODP Site 1263, Walvis Ridge)

Questa è la Versione finale referata (Post print/Accepted manuscript) della seguente pubblicazione:

Original Citation:

Microfossil evidence for trophic changes during the Eocene-Oligocene transition in the South Atlantic (ODP Site 1263, Walvis Ridge) / Bordiga, M; Henderiks, J.; Tori, F.; Monechi, S.; Fenero, R.; Legarda-Lisarri, A.; Thomas, E.. - In: CLIMATE OF THE PAST. - ISSN 1814-9324. - ELETTRONICO. - 11:(2015), pp. 1249-1270. [10.5194/cp-11-1249-2015]

Availability:

This version is available at: 2158/1070022 since: 2017-01-09T12:56:16Z

Published version:

DOI: 10.5194/cp-11-1249-2015

Terms of use:

Open Access

La pubblicazione è resa disponibile sotto le norme e i termini della licenza di deposito, secondo quanto stabilito dalla Policy per l'accesso aperto dell'Università degli Studi di Firenze (<https://www.sba.unifi.it/upload/policy-oa-2016-1.pdf>)

Publisher copyright claim:

(Article begins on next page)



Microfossil evidence for trophic changes during the Eocene–Oligocene transition in the South Atlantic (ODP Site 1263, Walvis Ridge)

M. Bordiga¹, J. Henderiks¹, F. Tori², S. Monechi², R. Fenero³, A. Legarda-Lisarri^{1,3}, and E. Thomas^{4,5}

¹Department of Earth Sciences, Uppsala University, Villavägen 16, 752 36 Uppsala, Sweden

²Dipartimento di Scienze della Terra, Università di Firenze, Via la Pira 4, 50121 Florence, Italy

³Departamento de Ciencias de la Tierra and Instituto Universitario de Investigación en Ciencias Ambientales de Aragón, Universidad de Zaragoza, Calle Pedro Cerbuna 12, 50009 Zaragoza, Spain

⁴Department of Geology and Geophysics, Yale University, New Haven, CT 06520, USA

⁵Department of Earth and Environmental Sciences, Wesleyan University, Middletown, CT 06459, USA

Correspondence to: M. Bordiga (manuela.bordiga@geo.uu.se)

Received: 17 April 2015 – Published in Clim. Past Discuss.: 7 May 2015

Revised: 27 August 2015 – Accepted: 7 September 2015 – Published: 30 September 2015

Abstract. The biotic response of calcareous nannoplankton to environmental and climatic changes during the Eocene–Oligocene transition was investigated at a high resolution at Ocean Drilling Program (ODP) Site 1263 (Walvis Ridge, southeast Atlantic Ocean) and compared with a lower-resolution benthic foraminiferal record. During this time interval, global climate, which had been warm under high levels of atmospheric CO₂ ($p\text{CO}_2$) during the Eocene, transitioned into the cooler climate of the Oligocene, at overall lower $p\text{CO}_2$. At Site 1263, the absolute nannofossil abundance (coccoliths per gram of sediment; N g^{-1}) and the mean coccolith size decreased distinctly after the E–O boundary (EOB; 33.89 Ma), mainly due to a sharp decline in abundance of large-sized *Reticulofenestra* and *Dictyococcites*, occurring within a time span of ~ 47 kyr. Carbonate dissolution did not vary much across the EOB; thus, the decrease in abundance and size of nannofossils may reflect an overall decrease in their export production, which could have led to variations in the food availability for benthic foraminifers.

The benthic foraminiferal assemblage data are consistent with a global decline in abundance of rectilinear species with complex apertures in the latest Eocene (~ 34.5 Ma), potentially reflecting changes in the food source, i.e., phytoplankton. This was followed by a transient increased abundance of species indicative of seasonal delivery of food to the sea floor (*Epistominella* spp.; ~ 33.9 – 33.4 Ma), with a short

peak in overall food delivery at the EOB (buliminid taxa; ~ 33.8 Ma). Increased abundance of *Nuttallides umbonifera* (at ~ 33.3 Ma) indicates the presence of more corrosive bottom waters and possibly the combined arrival of less food at the sea floor after the second step of cooling (Step 2).

The most important changes in the calcareous nannofossil and benthic communities occurred ~ 120 kyr after the EOB. There was no major change in nannofossil abundance or assemblage composition at Site 1263 after Step 2 although benthic foraminifera indicate more corrosive bottom waters during this time. During the onset of latest-Eocene–earliest-Oligocene climate change, marine phytoplankton thus showed high sensitivity to fast-changing conditions as well as to a possibly enhanced, pulsed nutrient supply and to the crossing of a climatic threshold (e.g., $p\text{CO}_2$ decline, high-latitude cooling and changes in ocean circulation).

1 Introduction

The late Eocene to early Oligocene was marked by an important change in global climate and in oceanic environments, reflected in significant biotic turnover. Earth's climate was driven from a warm “greenhouse” with high $p\text{CO}_2$ during the middle Eocene through a transitional period in the late Eocene to a cold “icehouse” at low $p\text{CO}_2$ in the earliest

Oligocene (e.g., Zachos et al., 2001; DeConto and Pollard, 2003; Pearson et al., 2009; Pagani et al., 2011; Zhang et al., 2013). During this climate shift, Antarctic ice sheets first reached sea level, sea level dropped, and changes occurred in ocean chemistry and plankton communities, while the calcite compensation depth (CCD) deepened rapidly, at least in the Pacific Ocean (e.g., Zachos et al., 2001; Coxall et al., 2005; Pälike et al., 2006; Coxall and Pearson, 2007; Merico et al., 2008). There is ongoing debate whether the overall cooling, starting at high latitudes in the middle Eocene while the low latitudes remained persistently warm until the end of the Eocene (Pearson et al., 2007), was mainly caused by changes in oceanic gateways (opening of Drake Passage and the Tasman gateway) leading to the initiation of the Antarctic Circumpolar Current (e.g., Kennett, 1977) or by declining atmospheric CO₂ levels that favored ice sheet growth (e.g., DeConto and Pollard, 2003; Barker and Thomas, 2004; Katz et al., 2008; Goldner et al., 2014) in combination with specific orbital configurations (Coxall et al., 2005) or by some combination of these factors (Sijp et al., 2014). Recently, it has been proposed that the glaciation itself caused further oceanic circulation changes (Goldner et al., 2014; Ladant et al., 2014; Rugenstein et al., 2014).

High-resolution benthic foraminiferal $\delta^{18}\text{O}$ records across the Eocene–Oligocene transition (EOT; ~ 34 – 33.5 Ma; Pearson et al., 2008) have shown a two-step cooling at several latitudes (e.g., Coxall et al., 2005; Katz et al., 2008; Lear et al., 2008; Coxall and Wilson, 2011; Bohaty et al., 2012). To avoid confusion with previous definitions of these two steps, we follow Pearson et al. (2008) and Bohaty et al. (2012): Step 1 is the first $\delta^{18}\text{O}$ increase related to global cooling with a modest ice growth component, and Step 2 is the second increase in $\delta^{18}\text{O}$ representing the major ice growth leading to a continental-scale ice sheet over Antarctica (Miller et al., 2009). Foraminifer-based geochemical studies documented the dynamics of the oceanic carbon cycle during the EOT, with an increase in benthic foraminiferal $\delta^{13}\text{C}$ which, on kiloyear timescales, could relate to an increased ratio in the burial of organic vs. inorganic carbon (calcite) due to enhanced marine export production and/or increased preservation of organic matter (e.g., Diester-Haass, 1995; Zachos et al., 1996; Coxall and Wilson, 2011). Enhanced export production, however, may not have been global (e.g., Griffith et al., 2010; Moore et al., 2014). The $\delta^{13}\text{C}$ shift and oceanic carbon cycle reorganization, linked to increased biological production and deepening of the CCD, have also been related to a rapid drop in $p\text{CO}_2$ (Zachos and Kump, 2005).

There is a strong link between late-Eocene–early-Oligocene climate change and the response of marine and terrestrial biota. The global cooling, with high extinction rates and ecological reorganization, affected many biological groups, including calcifying phytoplankton (coccolithophores; e.g., Aubry, 1992; Persico and Villa, 2004; Dunkley Jones et al., 2008; Villa et al., 2008), siliceous plankton (diatoms and radiolarians; e.g., Keller, 1986; Falkowski et

al., 2004), planktonic and benthic foraminifers (e.g., Coccioni et al., 1988; Thomas, 1990, 1992, 2007; Thomas and Gooday, 1996; Pearson et al., 2008; Hayward et al., 2012), large foraminifers (*Nummulites*; e.g., Adams et al., 1986), ostracods (e.g., Benson, 1975), marine invertebrates (e.g., Dockery, 1986), and mammals (e.g., Meng and McKenna, 1998). Among the marine biota, the planktonic foraminifers experienced a synchronous extinction of five species in the family Hantkeninidae (e.g., Coccioni et al., 1988; Coxall and Pearson, 2006), the extinction of *Turborotalia cerroazulensis* group and the reduction in size of the *Pseudohastigerina* lineage (Wade and Pearson, 2008, and references therein). Benthic foraminifers experienced a gradual turnover, marked by an overall decline in diversity, largely due to the decline in abundance of cylindrical taxa with a complex aperture (Thomas, 2007; Hayward et al., 2012), and an increase in species which preferentially use fresh phytodetritus delivered to the seafloor in strongly seasonal pulses (e.g., Thomas, 1992; Thomas and Gooday, 1996; Pearson et al., 2008).

Calcareous nannoplankton assemblages underwent significant global restructuring during the EOT, although the group did not suffer extinctions exactly at the Eocene–Oligocene boundary (EOB), in contrast with planktonic foraminifers. Calcareous nannoplankton flourished and diversified during the warm oligotrophic Eocene, with species diversity at maximum during the early to middle Eocene and decreasing during the cold eutrophic early Oligocene (Bown et al., 2004). Furthermore, coccolithophores were globally more common and widespread in the Eocene, distinctly declining in (common) occurrence since the early Oligocene (Hannisdal et al., 2012). Species diversity decreased at the expense of specialist taxa, favoring opportunistic species that were more adapted to the new environmental conditions (e.g., Persico and Villa, 2004; Dunkley Jones et al., 2008; Tori, 2008). The decline in diversity of nannoplankton since the middle Eocene coincided with a diversity increase in diatoms, which eventually outcompeted the nannoplankton as the dominant phytoplankton group (e.g., Spencer-Cervato, 1999; Bown et al., 2004; Falkowski et al., 2004).

In addition, the late Eocene to early Oligocene decrease in the average cell size of reticulofenestrids (ancestors of modern-day alkenone-producing coccolithophores *Emiliania huxleyi* and *Gephyrocapsa oceanica*) corresponds to a decline in $p\text{CO}_2$ (Henderiks and Pagani, 2008; Pagani et al., 2011). This macroevolutionary trend appears to have been global and primarily caused by the ecological decline in large reticulofenestrid species. Henderiks and Pagani (2008) hypothesized that large-celled coccolithophores were adapted to high $p\text{CO}_2$ and $\text{CO}_{2(\text{aq})}$ conditions (late Eocene), whereas small-sized species are more competitive at lower $p\text{CO}_2$ (early Oligocene). This hypothesis has not yet been tested in detail in the fossil record. Culture experiments, however, provide evidence that elevated levels of CO_2 alleviate carbon limitation in *E. huxleyi* and *G. oceanica* and that even these small-celled, bloom-forming coccolithophores oper-

ate carbon-concentrating mechanisms (CCMs) under today's natural conditions (e.g., Rost et al., 2003; Moolna and Rickaby, 2012). The adaptations in algal carbon acquisition due to lower $p\text{CO}_2$ may have occurred as late as during the late Miocene (about 7–5 Ma; Bolton and Stoll, 2013), suggesting that Paleogene coccolithophores did not (yet) operate CCMs and that diffusive uptake of CO_2 and growth rates were mainly determined by the volume-to-surface-area ratio of the cells.

To date, only few high-resolution studies describe the response of coccolithophores to environmental change along the EOT at high (Southern Ocean; Persico and Villa, 2004; Villa et al., 2008, 2014) and low latitudes (Tanzania; Dunkley Jones et al., 2008; Fioroni et al., 2015). These studies have highlighted distinct shifts in the composition of the assemblages and decreases in species diversity at or close to the boundary.

Here, we report on calcareous nannofossil and foraminiferal biotic events between 34.8 and 32.7 Ma at Ocean Drilling Program (ODP) Site 1263, in the southeast Atlantic Ocean. In particular, we refine the shipboard biostratigraphy published in Zachos et al. (2004), including new data on planktonic foraminifers, and describe the ecological response of calcareous nannoplankton and benthic foraminifers to environmental change during the EOT. The revealed distinct fluctuations in total abundance and taxonomic composition of the calcareous nannofossil assemblages are compared to stable isotope data (Riesselman et al., 2007; Peck et al., 2010) and to benthic foraminiferal assemblage data. For the first time, estimates of the number of nannofossils per gram of dry sediment are calculated for the Eocene–Oligocene time interval to evaluate how paleoexport fluxes and food supply to the benthic community were affected. This is also the first high-resolution (<10 000 years) record of coccolith size variations (and related changes in mean cell size; cf. Henderiks and Pagani, 2007) across the EOT.

2 Material and methods

2.1 ODP Site 1263

ODP Leg 208 Site 1263 (28°31.97' S, 2°46.77' E, Atlantic Ocean) was drilled at a water depth of 2717 m on the southern flank of Walvis Ridge, an aseismic ridge west of the African coast (Fig. 1). This site provides one of the most continuous sediment sequences of the lower Cenozoic in the Atlantic Ocean and was at least 1 km above the lysocline prior to the lowering of the CCD during the EOT (Zachos et al., 2004). Foraminifer-bearing nannofossil ooze and nannofossil ooze are the dominant lithologies in the studied interval (Zachos et al., 2004).

The Eocene–Oligocene sediments of ODP Site 1263 generally have a high carbonate content (CaCO_3 wt %), ranging from 88 to 96 % through 84.2–100.8 m composite

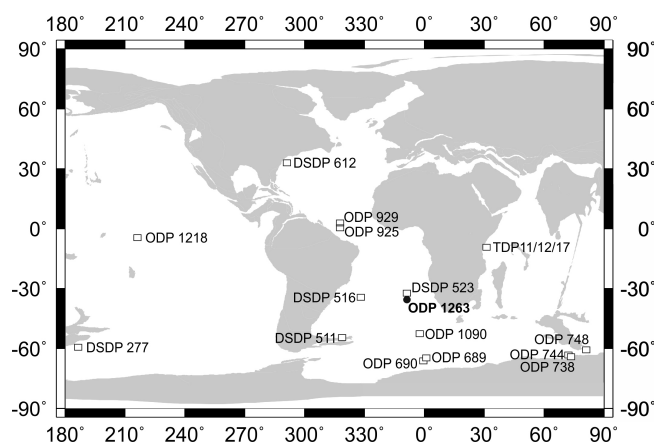


Figure 1. Paleogeographic reconstruction at 33 Ma (modified from Ocean Drilling Stratigraphic Network, Plate Tectonic Reconstruction Service, www.odsn.de/odsn/services/paleomap/paleomap.html) showing location of ODP Site 1263 (black dot) on Walvis Ridge. The positions of the other sites (white squares) used for comparison and cited in the text are also given.

depth (mcd; Riesselman et al., 2007). Only a few samples with lower values of CaCO_3 (~87 %) occur at 99.19 and 99.49 mcd (Riesselman et al., 2007).

A total of 190 samples was used for nannofossil analyses across the EOB. Two data sets, A and B, were independently produced at two laboratories and are here combined in a collaborative effort to also examine whether, and how, the primary nannofossil signals are consistently detected from the same sediment cores independent from sample spacing, microscopy slide preparation and operator. Data set A includes 114 samples from 83.19 to 101.13 mcd. The sampling resolution is high across the EOB (5–10 cm) and decreases above and below it: 20–90 cm between 83.19 and 89.6 mcd and 20–50 cm between 97.44 and 101.13 mcd. Data set B includes 76 samples (83.59–105.02 mcd, sampling resolution of 10–50 cm). For analyses on benthic foraminiferal assemblages, 27 samples between 80.89 to 109.79 mcd were used, while for planktonic foraminiferal analysis 16 samples between 93.42 and 107.29 mcd were studied (see Table S1 in the Supplement).

2.2 Microfossil preparation and assemblage counts

2.2.1 Nannofossils

Sample set A was prepared by weighing 5 mg of dried bulk sediment and diluting with 50 mL of buffered water. Then, 1.5 mL of well-mixed suspension was placed on a cover slip with a high-precision pipette, and the sample was dried on a hotplate at 60 °C. This technique (called the “drop technique” by Bordiga et al., 2015; modified after Koch and Young, 2007) avoids selective settling effects because the suspension volume is placed evenly on a cover slip and left

to settle and dry under low heat (see Bordiga et al., 2015, for details). Besides ensuring slides with an even particle distribution, this preparation technique also allows the calculation of the absolute coccolith abundances per gram of dry sediment (N g^{-1}). Repeated sample preparation and counting revealed a coefficient of variation (CV) of 6–10 % for absolute abundances (Bordiga et al., 2015), which is comparable to other techniques (e.g., Bollmann et al., 1999; Geisen et al., 1999). The drop method also provides a good reproducibility for the relative species abundances (Bordiga et al., 2015).

In this study we report on both absolute (N g^{-1}) and relative species abundances (%). Relative abundances are independent from sedimentological effects and estimates of sedimentation rate (e.g., Gibbs et al., 2012), but in contrast to absolute abundances, percentage values represent a closed sum, as each percentage value refers to how common or rare a species is relative to other species without knowing whether a species truly increased or decreased in absolute abundance. For these reasons a comparison of both is helpful to evaluate the influence of dilution and sedimentation rate variations and identify the real fluctuations in abundance of single species. Sample set B was prepared with the standard smear slide technique (Bown and Young, 1998), and the results are given as relative species abundances only.

In both data sets A and B, calcareous nannofossils were examined under polarized light microscopy (LM) at $1000\times$ magnification. At least 300 specimens were counted in each slide. Additional observations were carried out regarding the slide to detect the occurrence of rare species, especially biostratigraphical markers. All specimens were identified at species or genus level, depending on the coccolith preservation. We used *Cyclicargolithus* spp. to group the specimens with a dissolved central area that can be associated with the genus *Cyclicargolithus* but not directly with the species *Cyclicargolithus floridanus* (Fig. S1 in the Supplement). The taxonomy of the calcareous nannofossils follows the references found at the website <http://ina.tmsoc.org/Nannotax3> (edited by Young et al., 2014). Additional taxonomical remarks are given in the Supplement. For data set A, the number of fields of view (FOVs) observed were also noted in order to calculate absolute abundances. An average of 26 FOVs (0.31 mm^2) was observed along the sequence, from a minimum of 18 FOVs (0.21 mm^2) to a maximum of 44 FOVs (0.52 mm^2). Both data sets were used to provide biostratigraphical information: data set A with a more detailed resolution across the EOB and data set B covering a longer interval below the EOB.

2.2.2 Foraminifers

The samples were oven-dried at 60°C , then washed over a $63\text{ }\mu\text{m}$ sieve. The complete $>63\text{ }\mu\text{m}$ size fraction was used for the study of benthic foraminifers. Taxa were generally determined at species level (Fenero et al., 2010) and relative abundances were calculated. The benthic foraminiferal

studies were on the number of foraminifers in the full sample. All specimens were picked from material spread out in a picking tray, mounted on microslides for identification, then deposited at the Department of Earth Sciences, University of Zaragoza (Spain). The planktonic foraminiferal assemblages were observed in the $>63\text{ }\mu\text{m}$ fraction to determine the presence of biostratigraphical markers, such as the *Turborotalia cerroazulensis* group and species of the family Hantkeninidae. The presence or absence of tubulospines was noted (Table S1). The reduction in size of the *Pseudohastigerina* lineage was observed by counting the number of *Pseudohastigerina micra* and *Pseudohastigerina nagewichiensis* in a total of 300 planktonic foraminifers in the $150\text{--}250\text{ }\mu\text{m}$ and $125\text{--}150\text{ }\mu\text{m}$ fractions (cf. Wade and Pearson, 2008; Table S1).

2.3 Biotic proxies

2.3.1 Nannofossil dissolution index and cell size estimates

Sample set A was used to characterize nannofossil dissolution across the investigated interval. A coccolith dissolution index was calculated using the ratio between entire coccoliths and fragments (cf. Beaufort et al. 2007; Blaj et al., 2009; Pea, 2010). This index is indicative of the preservation or dissolution state of the nannofossil assemblages: higher values correspond to better preservation. Entire coccoliths and all fragments were counted until at least 300 entire coccoliths had been counted. Only pieces bigger than $3\text{ }\mu\text{m}$ were considered as fragments.

Mean coccolith and cell size estimates (volume-to-surface-area ratio, $V:SA$; cf. Henderiks and Pagani, 2007; Henderiks, 2008) were calculated based on the relative abundance and size range ($3\text{--}7$, $7\text{--}11$ and $11\text{--}16\text{ }\mu\text{m}$ for *Coccolithus*; $3\text{--}5$, $5\text{--}7$ and $7\text{--}9\text{ }\mu\text{m}$ for all the other species) of placolith-bearing taxa (*Coccolithus*, *Cyclicargolithus*, *Dictyococcites* and *Reticulofenestra*).

2.3.2 Calcareous nannofossil paleoecology

The distribution of coccolithophores in sea surface waters is controlled by the availability of light, temperature, salinity and nutrient availability (e.g., Winter et al., 1994). Studies of modern and past paleogeographic distributions of coccolithophores allow the determination of (paleo)environmental tolerances of various taxa (see Table 3 in Villa et al., 2008). However, some paleoecological interpretations remain unresolved or contradictory between different regions (see Table 3 in Villa et al., 2008). Therefore, we aimed to circumvent problems in interpretation by not tagging certain (groups of) species a priori but instead investigating the behavior within assemblages (see Sect. 2.4) and then comparing these with independent proxies (i.e., geochemical and benthic foraminiferal assemblage data).

2.3.3 The $\delta^{13}\text{C}$ gradient in foraminiferal tests

The difference between planktonic and benthic foraminiferal carbon isotope values ($\Delta\delta^{13}\text{C}_{\text{p-b}}$) was proposed as a semi-quantitative proxy of paleoproductivity (Sarnthein and Winn, 1990). It provides information about the surface to deep-water gradient in $\delta^{13}\text{C}$ in dissolved inorganic carbon (DIC), reflecting a combination of surface paleoproductivity and ocean circulation and stratification (e.g., Zhang et al., 2007; Bordiga et al., 2013). We calculated the $\Delta\delta^{13}\text{C}_{\text{p-b}}$ using data in Riesselman et al. (2007) and Peck et al. (2010).

2.3.4 Benthic foraminifers as paleoenvironmental proxies

We determined the relative abundances of benthic foraminiferal taxa and the diversity of the assemblages, expressed as the Fisher's alpha index (Hayek and Buzas, 2010). Changes in the relative abundances and diversity were used to infer changes in carbonate saturation state, oxygenation and food supply (e.g., Bremer and Lohmann, 1982; Jorissen et al., 1995, 2007; Gooday, 2003; Thomas, 2007; Gooday and Jorissen, 2012).

The relative abundance of infaunal benthic foraminiferal taxa has been linked to a combination of oxygenation and food supply (TROX model; Jorissen et al., 1995, 2007; Gooday, 2003), with high relative abundances reflecting a high food supply, extreme low oxygenation levels, or some combination of both. In addition, calcifying infaunal dwellers may gain an advantage over epifaunal dwellers during deep-water acidification (Foster et al., 2013). We have no sedimentological or stable isotope evidence for low-oxygen conditions, and the CaCO_3 percentage remains high over the studied interval (Riesselman et al., 2007). Therefore, we interpret a high relative abundance of the infaunal, triserial buliminids as indicative of a high, year-round food supply (Jorissen et al., 1995, 2007; Gooday, 2003). High relative abundances of phytodetritus-using taxa indicate an overall more moderate as well as a high (seasonal or episodic) flux of non-refractory particulate organic matter (e.g., Gooday, 2003; Jorissen et al., 2007). A high relative abundance of *Nuttallides umbonifera* indicates waters highly corrosive to CaCO_3 in generally low food supply settings (Bremer and Lohmann, 1982; Gooday, 2003).

Comparisons between past and recent benthic assemblages as indicators for features of deep-sea environments need careful evaluation because Eocene deep-sea benthic foraminiferal assemblages were structured very differently from those living today, and the ecology even of living species is not well known. For instance, in the Paleogene, taxa reflecting highly seasonal or episodic deposition of organic matter (phytodetritus) were generally absent or rare, increasing in relative abundance during the EOT (e.g., Thomas and Gooday, 1996; Thomas, 2007). At Walvis Ridge, these species did occur at much lower abundances during the EOT

after Eocene hyperthermal event 2 (Jennions et al., 2015), during the transition from early to middle Eocene (Ortiz and Thomas, 2015) and during the middle Eocene climatic optimum (MECO; Boscolo-Galazzo et al., 2015). During the time interval from the early to late Eocene through the EOT, their abundance thus increased overall, though episodically and with considerable fluctuations.

In contrast, in the Paleogene, cylindrically shaped taxa with complex apertures (called “Extinction Group” taxa by Hayward et al., 2012) were common (e.g., Thomas, 2007). These taxa globally declined in abundance during the increased glaciation of the earliest Oligocene and middle Miocene to become extinct during the middle Pleistocene (Hayward et al., 2012). The geographic distribution of these extinct taxa resembles that of buliminids but differs in detail (e.g., Hayward et al., 2012). These taxa were probably infaunal, as confirmed by their $\delta^{13}\text{C}$ values (Mancin et al., 2013). It is under debate what caused their Pleistocene extinction and decline in abundance across the EOB (Hayward et al., 2012; Mancin et al., 2013). Changes in the composition of phytoplankton, their food source, have been mentioned as a possible cause, as well as declining temperatures, increased oxygenation or viral infections (Hayward et al., 2012; Mancin et al., 2013).

2.4 Statistical treatment of the nannofossil data

Relative species abundances are commonly lognormally distributed (MacArthur, 1960). To generate suitable data sets for statistical analysis, different transformations yielding Gaussian distributions must be applied, such as log transformation (e.g., Persico and Villa, 2004; Saavedra-Pellitero et al., 2010), centered log ratio (e.g., Kucera and Malmgren, 1998; Buccianti and Esposito, 2004), and arcsine (e.g., Auer et al., 2014).

The nannofossil species percentages were used in the statistical treatment to compare the data sets A and B. Two transformations were tested: (i) log transformation by $\log(x+1)$, which amplifies the importance of less abundant species and minimizes the dominance of few abundant species (Mix et al., 1999), and (ii) centered log ratio (clr) transformation (Aitchison, 1986; Hammer and Harper, 2006), which opens a closed data matrix and retains the true covariance structure of compositional data. The normal distribution of each species before and after the transformations was verified using SYSTAT 13.0 software. Data sets A and B were treated the same but analyzed independently.

Principal component analysis (PCA) was performed on the transformed data using the statistics software PAST (Paleontological STatistic; Hammer et al., 2001). Species with an abundance of $< 1\%$ in all samples were not included in the PCA. The PCA (Q-mode) was performed to identify the major loading species and to evaluate the main factors affecting the changes on fossil coccolithophore assemblages.

The closed-sum problem, or constant-sum constraint, may obscure true relationships among variables (Pearson, 1896). The clr transformation has a major problem in carrying out the PCA on the covariance matrix, and the goal of keeping the most important data information with only few principal components (PCs) can fail using clr transformation in associations containing many outliers (e.g., Maronna et al., 2006), as is often the case in nannofossil assemblages. To minimize the presence of outliers, we worked with abundant species and groups of nannofossils instead of with single species.

The PAST software was also used to calculate the Shannon index, H , a diversity index taking into account a combination of evenness and diversity. High values indicate high evenness and/or high richness.

3 Biostratigraphy

The EOB at Site 1263 was tentatively placed between 83 and 110 mcd by the Leg 208 Shipboard Scientific Party (Zachos et al., 2004). Our high-resolution sampling allowed refining the position of the EOB by locating nannofossil and planktonic foraminiferal bioevents (Fig. 2; Table 1), including some bioevents not reported in Zachos et al. (2004).

The identified bioevents are delineated as “base” (stratigraphic lowest occurrence of a taxon), “top” (stratigraphic highest occurrence of a taxon), and “base common” (Bc, first continuous and relatively common occurrence of a taxon) following Agnini et al. (2014). No correlation with magnetostratigraphy was possible because the nannofossil oozes did not carry a clear signal (Zachos et al., 2004). The depths of all identified nannofossil and planktonic foraminiferal datums, together with the ages assigned to the most reliable datums as defined in Pälike et al. (2006) and Gradstein et al. (2012) are displayed in Table 1. Only one bioevent – the top of *Isthmolithus recurvus* – is not reported in Pälike et al. (2006); thus, we adopted the age given in Lyle et al. (2002; Table 1).

Based on the identified bioevents (see below for details), we documented that the studied succession runs from 32.7 Ma (top of *I. recurvus*; Lyle et al., 2002) to 34.77 Ma (top of *Discoaster barbadiensis*; Pälike et al., 2006). The estimated average sedimentation rate is 12 m myr^{-1} , close to the average value of $\sim 10.8 \text{ m myr}^{-1}$ in Zachos et al. (2004). In data set A, where the sample distribution is more homogeneous, the sampling resolution is $< 10\,000$ years across the EOT (from 97.29 to 90.02 mcd).

3.1 Calcareous nannofossils

The results from both data sets A (higher resolution) and B (longer time interval) render similar biostratigraphical evidence and well-constrained bioevents, especially for the rare species. Using the absolute and relative abundances of both data sets, we identified nine calcareous nannofossil datums (Fig. 2; Table 1). The studied interval runs from CNE20

(pars) Zone to CNO2 (pars) Zone in the recent biozonation of Agnini et al. (2014). The bioevents include

- base of *Sphenolithus tribulosus*, the lowermost datum identified (at 103.11 mcd, Table 1). We detected this species at the top of CNE20 Zone (Fig. 2), slightly below the range reported by Bown and Dunkley Jones (2006), who documented it between the NP21 and NP23 Zones (biozonation of Martini, 1971), corresponding to the CNE21–CNO4 Zones (Agnini et al., 2014). At Site 1263, this species is rare and sporadic, and poor preservation of the studied material compromises the identification at the species level and thus, possibly, its base.
- top of *Discoaster barbadiensis* and *Discoaster saipanensis*. The rosette-shaped discoasters at the bottom of the succession are usually well preserved without overgrowth (Fig. S1). The top of *D. barbadiensis* was not reported by the Shipboard Scientific Party (Zachos et al., 2004), and we placed this bioevent 1 m below the top of *D. saipanensis* (Fig. 2), identified by Zachos et al. (2004) 2 m below our datum (Table 1). We placed the top of *D. saipanensis* at 102.27 mcd because specimens of *D. saipanensis* had been continuously found until 102.52 mcd, although outside the count of 300 specimens (Fig. 2). These two bioevents were usually considered concurrent, but high-resolution studies (Berggren et al., 1995; Lyle et al., 2002; Tori, 2008; Blaj et al., 2009; Fioroni et al., 2015) show that they are shortly spaced. The top of *D. saipanensis* is used to define the CNE20–21 zonal boundary.
- base common of *Clausicoccus subdistichus*. We included *Clausicoccus obrutus* in the *C. subdistichus* concept following Agnini et al. (2014), although *C. obrutus* is the most abundant of the two species at Site 1263 (see Fig. S2). The absolute abundance variations together with the relative abundance in the more detailed data set A identify the Bc at 96.92 mcd, $\sim 2 \text{ m}$ below the depth reported by the Leg 208 Shipboard Scientific Party (94.77 mcd; Table 1; Fig. 2) and $\sim 60 \text{ cm}$ above the observed top of *Hantkenina* spp. and the reduction in size of *Pseudohastigerina* (Fig. 2; see the foraminifer section). The Bc of *C. subdistichus* defines the base of CNO1 (Agnini et al., 2014), which corresponds to the upper zone NP21 (Martini, 1971). The Bc of *C. subdistichus* (referred to as *C. obruta*) has been observed shortly after the EOB at Deep Sea Drilling Project (DSDP) Sites 522 and 523 in the SE Atlantic (Backman, 1987) – in the vicinity of Site 1263 – as well as in the Tethys Massignano Global Stratotype Section and Point (GSSP) and Monte Cagnero sections (Tori, 2008; Hyland et al., 2009), at high-latitude Site 1090 (Marino and Flores, 2002) and in the NW Atlantic (Norris et al., 2014).

Table 1. Calcareous nannofossil and planktonic foraminiferal (underlined) bioevents as identified in this study (at meter composite depth, mcd) and the mcd reported by the Shipboard Scientific Party (Zachos et al., 2004). Note that for the planktonic foraminiferal bioevents the average depth is reported. For each bioevent, the ages available in the most recent literature are given. N.A.: datum not available; *: ages not included in the sedimentation rate estimate.

Datum	This study	Shipboard Scientific Party (Zachos et al., 2004)		Ages (Ma)	References
	Interval (hole-core-section, cm)	Depth (mcd)	Average depth (mcd)		
T <i>Isthmolithus recurvus</i>	B-3H-5, 115–116	83.19	86	32.7	Lyle et al. (2002)
T <i>Coccolithus formosus</i>	A-9H-4, 9–10	85.16	86	32.92	Pälike et al. (2006)
Bc <i>Sphenolithus akropodus</i>	A-9H-4, 100–102	86.34	N.A.		
B <i>Chiasmolithus altus</i>	B-4H-2, 131–132	89.4	N.A.	33.31*	Pälike et al. (2006)
B <i>Sphenolithus akropodus</i>	B-4H-3, 50–52	90.09	N.A.		
Bc <i>Clausicoccus subdistichus</i>	A-10H-4, 141–142	96.92	94.77	33.88*	Pälike et al. (2006)
T <i>Hantkenina</i> spp.	A-10H-5, 32–34/B-4H, CC	97.53	104.5	33.89	Gradstein et al. (2012)
<u>Pseudohastigerina size reduction</u>	A-10H-5, 32–34/B-4H, CC	97.53	N.A.	33.89	Gradstein et al. (2012)
<u>T <i>Turborotalia cerroazulensis</i> group</u>	A-10H-5, 32–34/B-4H, CC	97.53	N.A.		
T <i>Discoaster saipanensis</i>	B-5H-3, 50–52	102.27	104.1	34.44	Pälike et al. (2006)
T <i>Discoaster barbadiensis</i>	B-5H-4, 0–2	103.27	N.A.	34.77	Pälike et al. (2006)
B <i>Sphenolithus tribulosus</i>	B-5H-4, 50–52	103.77	N.A.		

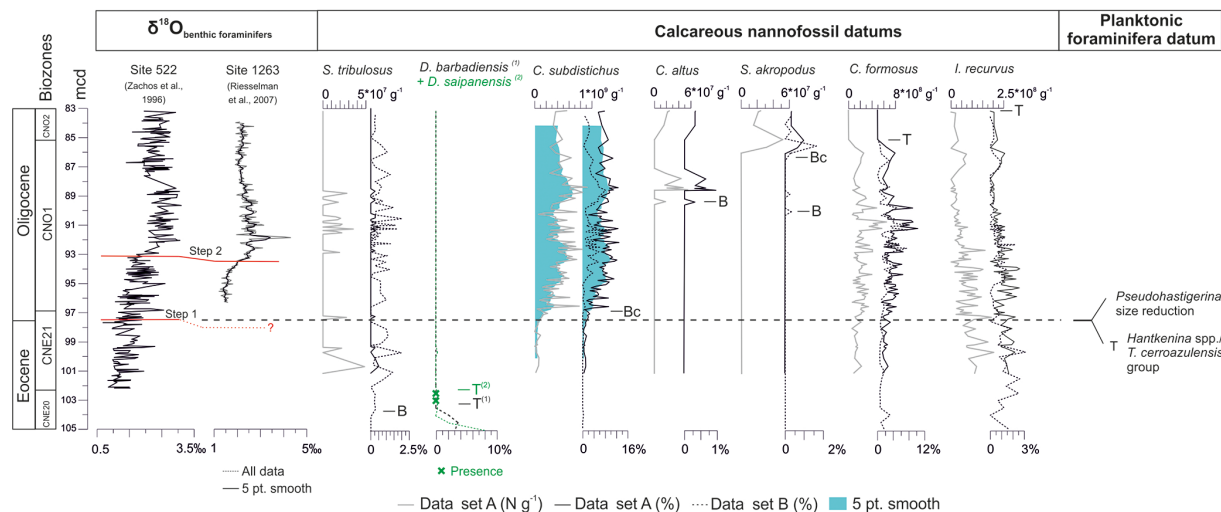


Figure 2. Eocene–Oligocene stratigraphy of Site 1263 and DSDP Site 522 (Walvis Ridge). Stable oxygen isotope stratigraphy ($\delta^{18}\text{O}$, ‰) at DSDP Site 522 (Zachos et al., 1996) compared to that at Site 1263 (Riesselman et al., 2007). Absolute abundances of nannofossil marker species (N g^{-1} ; note 10^7 – 10^8 – 10^9 change in scale among curves) for data set A (grey line) and their relative percentages (%) for data sets A (black line) and B (black dashed). A five-point smoothed curve is shown for the species *C. subdistichus*. Note the changes in horizontal scale among curves. Calcareous nannofossil and planktonic foraminiferal datums are highlighted. B: base occurrence; T: top occurrence; Bc: base common occurrence.

– base of *Chiasmolithus altus*. The rare and discontinuous presence of *C. altus* creates some bias in the detection of its base. Moreover, *C. altus* specimens are highly affected by dissolution as their central area is commonly completely dissolved (Fig. S1). The base of *C. altus* is tentatively placed at 89.4 mcd where a specimen with whole central crossbars meeting at 90° was observed (Fig. S1). At Site 1263, the base of *C. altus*, the youngest representative of the genus, falls inside the lower Oligocene (Zone CNO1; Fig. 2), as also docu-

mented in the NE Atlantic (de Kaenel and Villa, 1996) and at high latitudes (Persico and Villa, 2004; Villa et al., 2008).

– base and Bc of *Sphenolithus akropodus*. Rare sporadic occurrence and poor preservation affect the recognition of this species, but Bc was identifiable (Fig. 2; Table 1). We tentatively also delineated the base, but only few species were detected and they were sporadic (Fig. 2). The Bc is consistent with the identified datum reported in de Kaenel and Villa (1996), who used this bioevent

to approximate the Zone NP21/22 boundary and the top of *Coccolithus formosus*.

- top of *Coccolithus formosus*. This bioevent was easily detectable, as *C. formosus* is abundant and well preserved. Its top defines the CNO1–CNO2 zonal boundary (Fig. 2), close to the depth suggested onboard ship (Table 1).
- top of *Isthmolithus recurvus*, the highest datum identified (Fig. 2). Its abundance is low, so that its distribution becomes discontinuous towards the top of the studied interval. The 83.19 mcd depth (Table 1), 3 m above that reported by the Shipboard Scientific Party (Zachos et al., 2004), is an approximation because just one sample above the highest observed specimens of *I. recurvus* was analyzed.

3.2 Planktonic foraminifers

The Eocene–Oligocene boundary (EOB; ~ 33.89 Ma; Gradstein et al., 2012) is denoted at its GSSP at Massignano in Italy by the extinction of the family Hantkeninidae (specifically of species in the genera *Hantkenina* and *Cribohantkenina*; Premoli Silva and Jenkins, 1993). Unless well-preserved material is available (as for, e.g., the Tanzania Drilling Project (TDP) sites; Pearson et al., 2008), the sensitivity of hantkeninids to fragmentation and dissolution may lead to a misplacement of the family's true highest occurrence. At several well-studied sites, for example ODP Site 744 (Zachos et al., 1996) and Site 1218 (Coxall et al., 2005), hantkeninids are not present. In such cases, additional planktonic foraminifer bioevents must be considered to identify and correlate the EOB between sites: (i) the extinction of the *Turborotalia cerroazulensis* group which preceded the EOB (Berggren and Pearson, 2005; Pearson et al., 2008) and (ii) the reduction in size of the *Pseudohastigerina* lineage which occurred at the EOB (Wade and Pearson, 2008, and references therein).

At Site 1263, planktonic foraminifers are abundant and their preservation is generally good to moderate. Samples from 109.79 to 99.97 mcd, however, contain strongly fragmented planktonic foraminifers, with non-broken specimens dominated by heavily calcified *Globigerinatheca* spp. (Zachos et al., 2004). Unfortunately, species of the hantkeninid group are not well preserved and occur as fragments of variable size, including tubulospines and partial specimens (several chambers). Entire or partially preserved specimens of hantkeninids as well as loose tubulospines have been observed from the bottom sample (107.29 mcd) up to 97.91 mcd. No specimen of *Hantkenina* spp. nor even tubulospine were seen from 97.14 mcd upward (Table S1). Therefore, we focused on the top of the *T. cerroazulensis* group (comprising *T. cerroazulensis*, *T. cocoaensis*, and *T. cunialensis*) and the size reduction of the *Pseudohastigerina*

lineage, characterized as the top of > 125 μm -sized *Pseudohastigerina micra*. These two bioevents were detected at the same depth as the top of *Hantkenina* spp., i.e., the three bioevents all fall in between 97.91 and 97.14 mcd (Fig. 2; Table S1). Due to the lower resolution of the sampling for planktonic foraminifers than for nannofossils, the three bioevents may not be exactly coeval but occur at that interval of less than 1 m (~ 70 kyr). Nevertheless, we can refine the position of the EOB reported in Zachos et al. (2004), where only core catcher samples were studied and place the EOB between 97.91 and 97.14 mcd, i.e., at 97.53 mcd (Fig. 2). This position of the EOB is in agreement with the nannofossil bioevent, Bc of *C. subdistichus*, just above that level (96.92 mcd; see Sect. 3.1).

A further confirmation of this placement of the EOB comes from the benthic foraminifer oxygen isotope data. The EOB occurs between the two main steps in $\delta^{18}\text{O}$ characterizing the EOT cooling and glaciation at TDP Sites 12 and 17, where assemblages are pristine (Pearson et al., 2008). At Site 1263, high-resolution $\delta^{18}\text{O}$ data are available only from 96 mcd up. Step 2 is identifiable at 93.4 mcd, at the maximum value of benthic $\delta^{18}\text{O}$ (Fig., 2; Riesselman et al., 2007; Peck et al., 2010). Step 1 was tentatively placed by Peck et al. (2010) at ~ 93.8 mcd, but the $\delta^{18}\text{O}$ curve does not reveal a signal of the first cooling step as clearly as at Pacific Site 1218 (Coxall et al., 2005) and nearby Site 522 at Walvis Ridge (Zachos et al., 1996; Coxall and Wilson, 2011). We argue that Step 1 should be placed below 97.53 mcd at Site 1263, not only on the basis of the planktonic foraminiferal and nannofossil bioevents but also by comparison with the oxygen isotope curve at Site 522, which records a complete and clear $\delta^{18}\text{O}$ signal for the entire EOT (Fig. 2). The two sites are geographically close and have comparable sedimentation rate across the EOT (12 m myr^{-1} at Site 1263; 9 m myr^{-1} at Site 522, Hsü et al., 1984). Because Step 1 and Step 2 occur within ~ 4 m at Site 522 (Zachos et al., 1996; Coxall and Wilson, 2011), we can infer that a similar pattern is present at Site 1263, placing Step 1 between 97.5 and 98.5 mcd (Fig. 2). A $\delta^{18}\text{O}$ signal similar to the one at Site 522, with Step 1 placed ~ 2 m below the EOB, is recorded at Site 1265 on the Walvis Ridge (lower sampling resolution; sedimentation rate 5.7 m myr^{-1} ; Liu et al., 2004). This evidence does not agree with the previous proposed position for Step 1 at only 40 cm below Step 2 (Peck et al., 2010). More oxygen isotope analyses are necessary to definitely place Step 1 in the sediment column at Site 1263.

4 Biotic responses

4.1 Calcareous nannofossil preservation and assemblages

At ODP Site 1263 the carbonate content did not increase above the EOB (Fig. 3; Riesselman et al., 2007), in contrast to other sites, specifically in the Pacific Ocean (e.g.,

Salamy and Zachos, 1999; Coxall et al., 2005; Coxall and Wilson, 2011). This lack of response is probably due to the location of Site 1263 well above the lysocline since the late Eocene (Zachos et al., 2004), so that CaCO_3 (wt %) was and remained generally high and was not affected by CCD deepening (Fig. 3; Riesselman et al., 2007). The deeper Site 1262, close to Site 1263, was below the lysocline before the rise in CCD and shows a strong increase in CaCO_3 (wt %) across the EOB (from ~ 5 to > 90 %; Liu et al., 2004).

However, the CaCO_3 (wt %) at Site 1263 does not reflect the total coccolith absolute abundance (Fig. 3). This supports the idea that other calcifying organisms (mainly planktonic foraminifers) contributed consistently to the calcite accumulation in the sediments. To unravel the “true” contribution of each calcifying group to the accumulated CaCO_3 (wt %), we need to know the total amount of carbonate produced by calcareous nannoplankton and foraminifers, which is beyond the scope of this study.

Although the site was above the lysocline during the studied time interval, the nannofossil and foraminiferal assemblages show signs of dissolution throughout the sequence. Dissolution may occur above the lysocline (e.g., Adler et al., 2001; de Villiers, 2005), leading to a reduction in species numbers and an increase in fragmentation with depth, in both nannoplankton (e.g., Berger, 1973; Milliman et al., 1999; Gibbs et al., 2004) and planktonic foraminiferal assemblages (e.g., Peterson and Prell, 1985).

At Site 1263 signs of dissolution were detected, in particular, in specimens of *Cyclicargolithus* (Fig. S1) – one of the least resistant nannoplankton species (Blaj et al., 2009) – but also in more robust species such as *Dictyococcites bisectus*. Despite these signs, holococcoliths and abundant small- to medium-sized *Cyclicargolithus* – which are prone to dissolution (Young et al., 2005; Bown et al., 2008; Blaj et al., 2009) – are present in all samples. We did not see small placoliths ($< 3 \mu\text{m}$) at Site 1263, possibly due to dissolution, but these were not dominant in the late Eocene (e.g., Persico and Villa, 2004; Villa et al., 2008; Fioroni et al., 2015). The lack of such placoliths does not prevent the identification of the main features of the medium- to large-sized taxa.

Our coccolith dissolution index does not show any major changes across the EOT (91–98.5 mcd), but at 90.2 mcd and from 87 mcd upward nannofossil dissolution slightly increased (Fig. 3). The correlation between the dissolution index and total coccolith abundance is positive (entire interval $r = 0.32$; p value = 0) and stronger in the upper interval of the studied sequence ($r = 0.59$; p value = 0.002) but not significant across the EOB. Intervals of increased dissolution do not necessarily correspond to lower absolute abundances, so that we can infer that primary signals of the nannoplankton are preserved in the fossil assemblages at least across the EOB, with the exception of the primary presence or absence of small specimens.

Nannofossil diversity, as expressed in the H index, does not vary significantly across the EOB but decreases gradu-

ally within 1.5 m above the EOB. A more distinct stepwise decrease at 90 mcd (Fig. 3) reflects a community structure with fewer dominant species, possibly due to increased dissolution in this interval. Actually, *Cyclicargolithus* became dominant in this interval, while large *Reticulofenestra* decreased significantly in abundance (Fig. 3). The calcareous nannofossil assemblage variations recorded in sample sets A and B are comparable despite the different sampling resolution (Figs. S2 and S3). The trends in absolute and relative abundances are very similar (Fig. S2). Thus, we conclude that the dilution and sedimentation rates at Site 1263 were close to constant over time and that the variations in absolute abundance were linked to biological processes. Total absolute coccolith abundances show a marked decrease ~ 1.5 m above the EOB (Fig. 3): within 60 cm (from 96.39 to 95.79 mcd) the abundance rapidly drops by 45 %, mainly driven by the loss of large-sized species, including *D. bisectus*, *Dictyococcites stavensis*, *Reticulofenestra umbilicus*, *Reticulofenestra samodurovii*, *Reticulofenestra hillae*, and *Reticulofenestra circus* group (see taxonomical remarks in the Supplement). Among these, *D. bisectus* and *D. stavensis* constitute a significant part (up to 28 %) of the assemblage. The medium-sized *Reticulofenestra daviesii* also shows a decrease ~ 1.5 m above the EOB, contrary to what was reported at ODP Site 744 (Persico and Villa, 2004), Site 748 (Villa et al., 2008), Site 711 (Fioroni et al., 2015), and Site 1090 (Pea, 2010) for the same time interval. The small to medium *Cyclicargolithus* spp. and *C. floridanus* are the most abundant species (up to 50 %), and the 5–7 μm size group is dominant. This group increases slightly from the bottom upwards, and just above the EOB it records an increase in abundance. *Coccolithus pelagicus* is another important component of the nannofossil assemblage, at a maximum abundance of 27 % (Fig. 3). This species increases in abundance between 96.92 and 92.6 mcd, i.e., above the EOB, and then it decreases from 88 mcd upwards. *Sphenolithus* spp. does not show any marked variation at the EOB, even if this group is not very abundant. The increase in *Cyclicargolithus* and *C. pelagicus* does not coincide with the marked decrease in large reticulofenestrids indicating that the loss of the latter group was not compensated for by other taxa. The total coccolith abundance (and export production) thus decreased above the EOB.

Another component of the assemblage, *Lanternithus minutus*, is generally not abundant, but peaks between 89.6 and 87.12 mcd. *Zygrhablithus bijugatus* and *Discoaster* spp. both decreased in abundance below the EOB (at 98 and 99 mcd, respectively), and higher up in the section they never reached abundances as high as in the upper Eocene (Fig. 3).

4.1.1 Principal component analysis

Results from the PCAs performed on data sets A and B are comparable, both using the log or clr transformation. For data set A, the Pearson correlation value (r) between the compo-

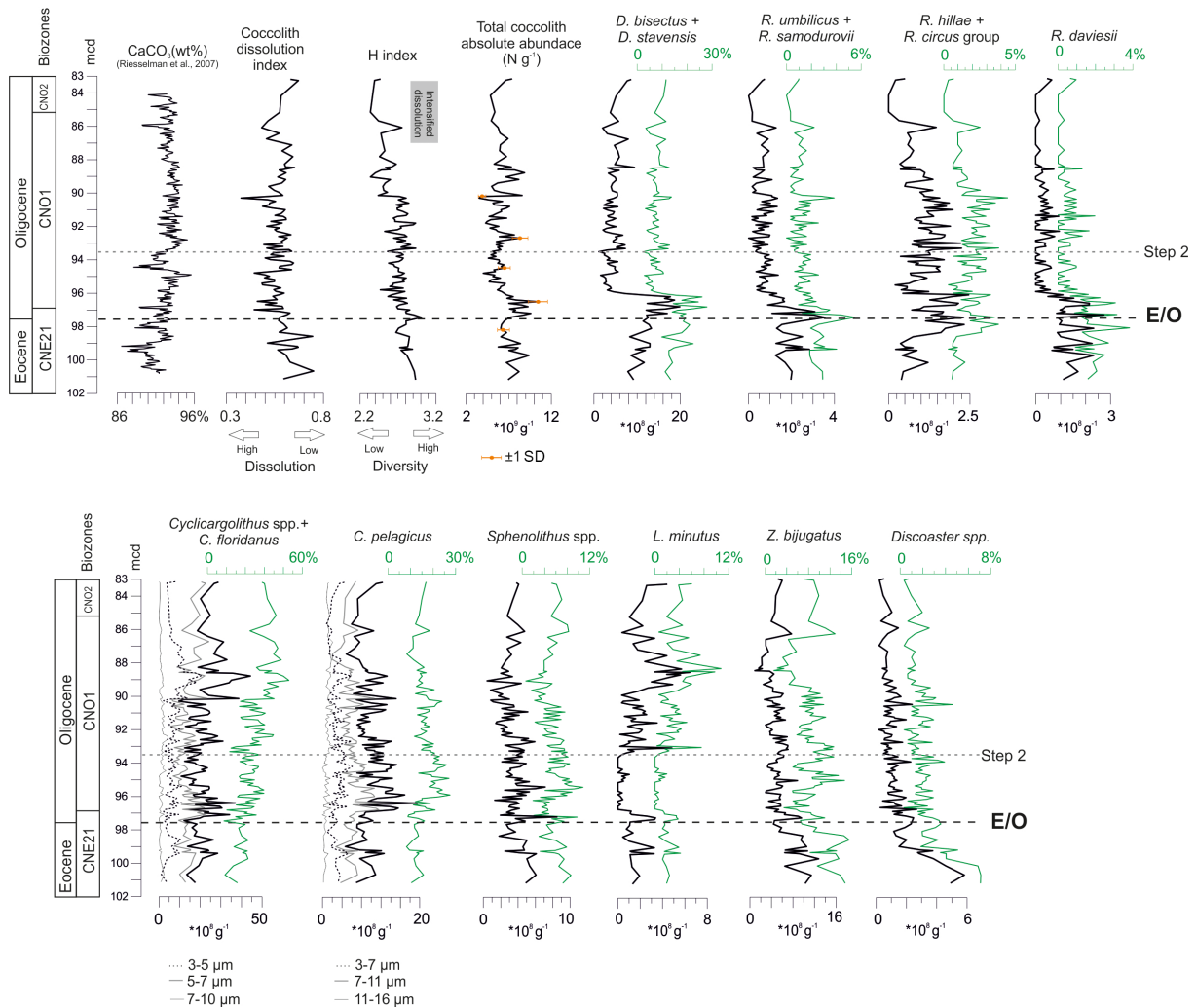


Figure 3. Calcareous nannofossil abundance and distribution against depth (mcd) at Site 1263 (data set A). CaCO_3 (wt %; Riesselman et al., 2007), coccolith dissolution index (%), H index, and the total absolute coccolith abundance (N g^{-1}). Error bars indicate the standard deviation (± 1 SD, in %) of replicate counts. The absolute (N g^{-1} , black line) and relative (% , green line) abundances of the main species constituting the assemblage are shown. For *Cyclocargolithus* spp. and *C. pelagicus* the absolute abundances of different size groups are shown. The grey vertical bar marks an interval of major dissolution (87 to 83 mcd). The positions of EOB and Step 2 are reported.

nents of the two transformations is 0.90 (p value = 0), confirming that the primary signals in the assemblage are reflected in the multivariate statistical analysis, as long as normal distribution of the species is maintained. We also compared the PCA results with or without the presence of the marker species because stratigraphically controlled species are not distributed along the entire succession, thus affecting PCA outcomes (e.g., Persico and Villa, 2004; Maiorano et al., 2013). The results obtained with and without the marker species provide similar trends for both data sets because in the studied interval the marker species are not very abundant (Fig. 4; Table S2).

In the following discussion, we will focus on the PCA results and the loading species using the log transformation for data sets A and B (Fig. 4; Tables S2 and S3). The only

two significant principal components explain 50 % of the total variance in data set A and account for 36 and 14 %. For data set B the two components explain 35 % (26 and 11 % respectively).

Principal component 1 (PC1) of data set A shows positive values below 96 mcd. A pronounced decrease occurs 1.5 m above the EOB, and from 96 mcd upwards the PC1 maintains mainly negative values (Fig. 4a). PC1 is negatively loaded by *C. obrutus* and small- and medium-size *C. floridanus* and positively by *D. stavensis*, *D. bisectus*, *R. daviesii*, and *R. umbilicus* (Fig. 4a; Table S2). The loadings of the other species are too low to be significant. The PC1 of data set B does not record the same marked drop above the boundary but rather a gradual decrease along the whole sequence (Fig. 4a). Although the main loading species are the same

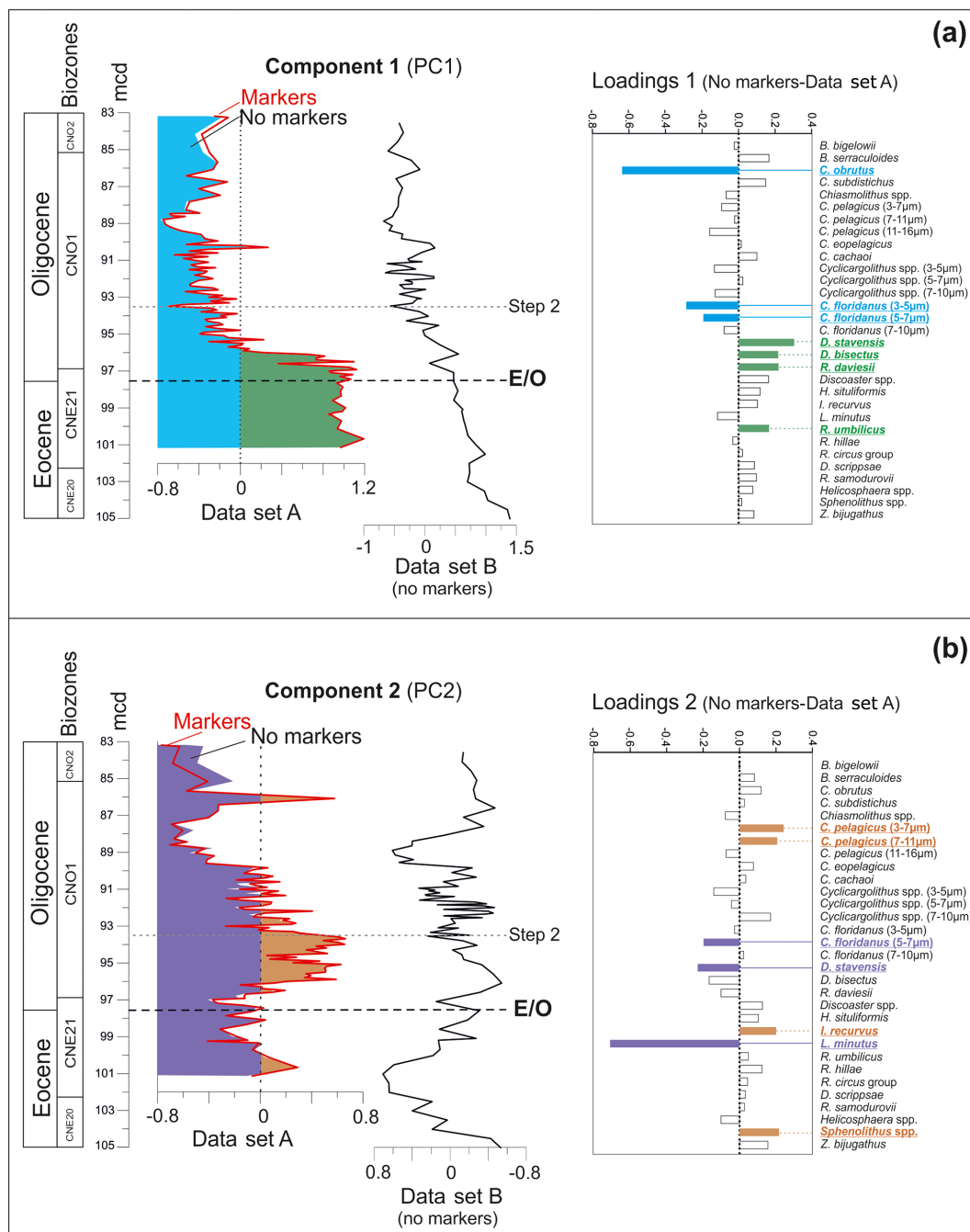


Figure 4. Distribution patterns of PC1 (a) and PC2 (b) obtained from the PCA for the data sets A and B. Loadings of calcareous nannofossil taxa on the two principal components of the whole studied succession for data set A are reported. The shaded boxes represent the most relevant loaded species. Shaded area: PCs (data set A) obtained omitting the marker species in the data set. Red line: PCs (data set A) obtained inserting also the marker species. The positions of EOB and Step 2 are reported.

for both data sets (i.e., *C. obrutus* and *Cyclicargolithus* versus *D. bisectus* and *R. umbilicus*), there are some differences (Tables S2 and S3). Specifically, the size groups of *Cyclicargolithus* do not influence PC1 in data set B because the size subdivision was not included in the counts of that data set. As the distribution of large- vs. small- to medium-sized species on the PCA seems to be important for both data sets and *Cyclicargolithus* is one of the most abundant species, the lack of a detailed size grouping within this genus in data set B might be the cause of the difference in the PC1 curves above the EOB. The higher abundances of *Discoaster* and *R. umbilicus* from the bottom up to 102 mcd in data set B could also explain some differences in the loading species between the two data sets (Tables S2 and S3 and Fig. S3).

Principal component 2 (PC2) of data set A also records an abrupt variation above the EOB (at 96 mcd): the negative values at the bottom of the succession turn toward positive values above the boundary, remaining positive up to 89.95 mcd. From 90 mcd upwards, PC2 displays mainly negative values, except for a peak between 85.68 and 86.42 mcd (Fig. 4b). The most meaningful species loading on PC2 is *L. minutus* (negative loading). The PC2 is also loaded negatively by *D. stavensis* and *C. floridanus* (5–7 μm) and positively by *C. pelagicus* (3–7 and 7–11 μm), *I. recurvus* and *Sphenolithus* spp. (Fig. 4b; Table S2). The PC2 for data set B shows a trend similar to that for data set A from 98 mcd upward (Fig. 4b), but it differs distinctly in the lower part of the succession. Again, the PC2 is resolved by the same main loading species *L. minutus* versus *C. pelagicus*, but the relative direction (positive or negative) of the loadings is reversed between data sets A and B (Tables S2 and S3). In particular, *L. minutus* has very strong loadings in both data sets. In data set B, *L. minutus* has its maximum abundance in the upper Eocene interval not sampled in data set A (Figs. S2 and S3), likely driving the differences between the two PC2 curves below the EOB (Fig. 4b).

In the following discussion, we only used the PCA results for data set A (without marker species) because of its more even sample distribution and direct comparison to the other available nannofossil proxies, i.e., dissolution index, coccolith size distribution and absolute abundance.

4.2 Mean coccolithophore cell size variations

The PC1 curve is mirrored ($r = 0.79$; p value=0) by mean cell size estimates ($V : SA$ ratio) of all medium- to large-sized ($> 3 \mu\text{m}$) placolith-bearing coccolithophores within the assemblages and of those of all ancient alkenone producers combined (i.e., *Cyclicargolithus*, *Reticulofenestra* and *Dictyococcites*; Planck et al., 2012) (Fig. 5). Fluctuations in mean size are mainly driven by the relative abundance of the different placolith-bearing taxa and their respective size groups rather than by intraspecific size variations. The mean $V : SA$ ratios were higher (species with large cells were more abundant) during the latest Eocene and early Oligocene, and the

size decreased (due to the loss of large species) by 8 % between 96.39 and 95.79 mcd (within ~ 47 kyr), which is, according to our age model, ~ 120 kyr after the EOB.

The coccolith dissolution index confirms that preferential dissolution did not bias the $V : SA$ results, as intervals of increased dissolution did not generally correspond to large $V : SA$ ($r = -0.12$). The only exception is the top, 90–90.3 mcd, interval where a high dissolution peak corresponds to an increase in mean size. In either case, the above $V : SA$ considerations do not include small placoliths ($< 3 \mu\text{m}$), so that our analysis is free from any bias due to the (original) presence or absence of this most dissolution-prone group.

4.3 Benthic foraminiferal assemblage

Benthic foraminifers show partial dissolution or etching, especially between 94.42 and 109.79 mcd, but are generally well preserved, i.e., sufficient for determination at species level (Fenero et al., 2010). The low-resolution data on benthic foraminifers show that the diversity of the assemblages (Fisher's alpha index curve; Fig. 6) started to decline in the late Eocene (~ 34.5 Ma; 102.79 mcd), reached its lowest values just below the EOB, then slowly recovered, but never to its Eocene values (Fenero et al., 2010). The decline in diversity was due in part to a decline in relative abundance of the generally rare but species-rich group of rectilinear species with complex apertures (Extinction Group species). Such a decline is observed globally at the end of the Eocene (Thomas, 2007; Hayward et al., 2012). The declining diversity (decreased evenness) was also due to a transient increase in the abundance of species indicative of seasonal delivery of food to the sea floor (phytodetritus species, mainly *Epistominella* spp.; ~ 33.9 – 33.4 Ma; 97.91–91.91 mcd), with a short peak in overall, year-round food delivery above the EOB (buliminid taxa; ~ 33.8 Ma; 96.41–96.27 mcd). From ~ 3 m above Step 2 (~ 33.3 Ma; 90.41 mcd) up, the abundance of *N. umbonifera*, an indicator of carbonate corrosive bottom waters, increased. Due to this evidence for dissolution, benthic foraminiferal accumulation rates cannot be used to estimate food supply quantitatively and reliably throughout the studied interval.

Evidence for effects of dissolution on benthic foraminiferal assemblages is seen in the interval where *N. umbonifera* is common, but not in the interval with peak abundance of phytodetritus species (thin-walled, solution-sensitive species) and the interval where buliminids peak. These intervals are also not recognized as influenced by carbonate corrosivity in the pore waters (Riesselman et al., 2007). Thus, we conclude that the increased percentage of infaunal taxa is, in this studied section, not due to dissolution, although such an effect is seen in sections with much more severe dissolution effects, such as the Paleocene–Eocene interval of ocean acidification (Foster et al., 2013). Increased abundance of buliminid taxa (though not of phytodetritus taxa) could possibly result from lowered-oxygen

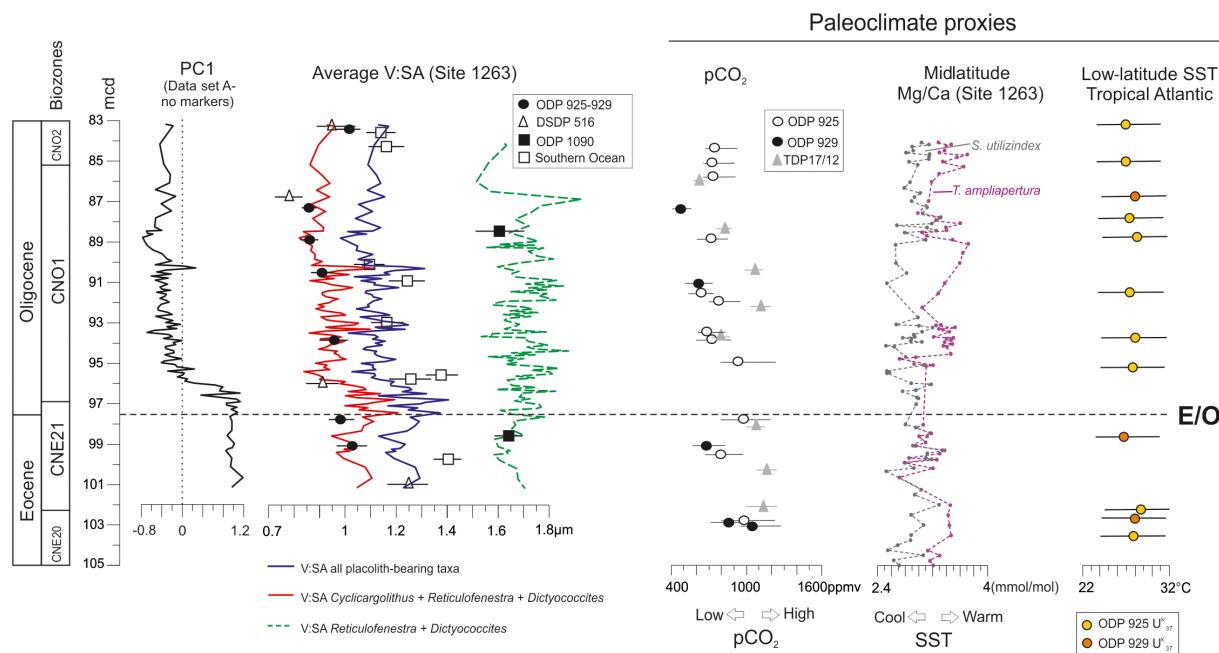


Figure 5. PC1 and cell size trends during the Eocene to Oligocene at Site 1263. The average cell $V : SA$ (μm) of all placolith-bearing species (green area), *Reticulofenestra*, *Dictyococcites* and *Cyclicargolithus* (red solid line) and *Reticulofenestra* and *Dictyococcites* (green dotted line) are reported. The average cell $V : SA$ of ODP 925 (black circles; Pagani et al., 2011), DSDP 516 (white triangles; Henderiks and Pagani, 2008), DSDP 511–277 (white squares) and ODP 1090 (black squares) from the Southern Ocean (Pagani et al., 2011), and alkenone-based $p\text{CO}_2$ (ppmv) from ODP 925 (white circles; Pagani et al., 2011; Zhang et al., 2013), ODP 929 (black circles; Pagani et al., 2011), and boron-isotope-based $p\text{CO}_2$ from TDP17/12 (grey triangles; Pearson et al., 2009) are also shown. For comparison with sea surface temperature (SST) proxies, the Mg/Ca (mmol mol^{-1} ; Peck et al., 2010) at Site 1263 and the SST from U_{37}^k at a low latitude in the Atlantic Ocean (Liu et al., 2009) are also displayed. The positions of EOB and Step 2 at Site 1263 are reported.

conditions in bottom or pore waters (e.g., Jorissen et al., 2007). However, there are no indications in the sediment of low-oxygen conditions (e.g., lamination), and the overall benthic assemblage does not indicate low-oxygen conditions (e.g., the diversity is too high).

5 Discussion

5.1 Nannoplankton abundance and cell size decrease after the EOB

The distinct variation in nannoplankton abundance and average size of medium to large placoliths above the EOB at Site 1263 cannot be explained by dissolution – which would affect smaller coccoliths preferentially and lead to an increase in the mean size of the whole assemblage, opposite to what is observed. It can also not be explained by a change in species diversity but is mainly linked to changes in community structure (Fig. 3). The drop in total nannofossil abundance (Fig. 3) and mean cell size (Fig. 5) is mainly driven by the decrease in abundance of large *Reticulofenestra* and *Dictyococcites* 1.5 m (~ 120 kyr) above the EOB. The mean $V : SA$ estimates for all ancient alkenone producers combined (i.e., *Cyclicargolithus*, *Reticulofenestra* and

Dictyococcites; Plancq et al., 2012) overlap tightly (Fig. 5) with biometric data of the same group in the equatorial Atlantic (Ceara Rise, ODP Sites 925 and 929; Pagani et al., 2011; Zhang et al., 2013), while the mean size estimates for combined *Reticulofenestra* and *Dictyococcites* remained relatively stable and coincide with mean values measured at ODP Site 1090 in the subantarctic Atlantic, where *Cyclicargolithus* spp. were not present and assemblages are likely severely affected by dissolution (Pea, 2010; Pagani et al., 2011). This highlights that the observed patterns in average placolith size at Site 1263 are driven by the decrease in abundance rather than (intraspecific) size variations of *Reticulofenestra* and *Dictyococcites*.

The assemblages also illustrate the midlatitude location of Site 1263, hosting both “subantarctic” and “equatorial” taxa. A striking correspondence between the mean $V : SA$ of ancient alkenone producers at Site 1263 and Sites 929 and 925 (Fig. 5) would suggest more affinity with tropical assemblages than with high-latitude ones, south of the subtropical convergence (STF). The abundance patterns of the larger reticulofenestrads, however, are more similar to those at Southern Ocean sites (Persico and Villa, 2004; Villa et al., 2008). The midlatitudinal Site 1263 thus probably records paleobiogeographic patterns in the nannofossil assemblage

intermediate between those in equatorial tropical and sub-antarctic regions.

The coccolith size shift and the decreased abundance of large reticulofenestrids after the EOB may be related to different bio-limiting factors. Under growth-limiting environmental conditions, phytoplankton (coccolithophores) with small cell-volume-to-surface-area ratios may outcompete larger cells due to lower resource requirements (lower C, P and N cell quota) and generally higher growth rates (e.g., Daniels et al., 2014). A change in overall nutrient regime, such as in coastal upwelling vs. oligotrophic, stratified gyre systems, may also cause a shift in opportunistic vs. specialist taxa (e.g., Falkowski et al., 2004; Dunkley Jones et al., 2008; Henderiks et al., 2012). The 16–37 % absolute abundance declines in the reticulofenestrid species *R. umbilicus*, *R. samodurovii*, *R. hillae* and *R. circus* group (Figs. 3 and S2) are strong indications that these large-celled coccolithophores were at a competitive disadvantage already during or shortly after the EOB. Earlier biometric studies of reticulofenestrid coccoliths point to a similar scenario (Fig. 5), postulating that the macroevolutionary size decrease reflects the long-term decline in $p\text{CO}_2$ (Henderiks and Pagani, 2008; Pagani et al., 2011; Hannisdal et al., 2012). High CO_2 availability during the late Eocene could have supported high diffusive CO_2 -uptake rates and photosynthesis even in the largest cells, assuming that Paleogene coccolithophores had no or an inefficient CO_2 -concentrating mechanism, similar to modern species today (Rost et al., 2003; Bolton and Stoll, 2013) and due to the fact that RuBisCo specificity for CO_2 increases at higher CO_2 levels (Giordano et al., 2005).

Available paleo- $p\text{CO}_2$ proxy reconstructions from equatorial regions (Pearson et al., 2009; Pagani et al., 2011; Zhang et al., 2013) indicate a transient decrease in $p\text{CO}_2$ across the studied interval rather than a distinct drop in $p\text{CO}_2$ after the EOB, which appears to be supported by our high-resolution assemblage (PC1) and mean $V : \text{SA}$ time series (Fig. 5). The paleo- $p\text{CO}_2$ proxy data, however, are at a much lower time resolution, based on a range of geochemical proxies and assumptions (Pearson et al., 2009; Pagani et al., 2011; Zhang et al., 2013). Therefore, they may not record the drop in $p\text{CO}_2$ as accurately as our comparative analysis would require. The range of estimated $p\text{CO}_2$ values is fairly wide: mean values are 940 ppmv before the EOB (SD range 740–1260 ppmv) and 780 ppmv after the boundary (SD range 530–1230 ppmv; Pearson et al., 2009; Pagani et al., 2011; Zhang et al., 2013; Fig. 5).

Possibly, shortly after the EOB a threshold level in $p\text{CO}_2$ was reached, below which large reticulofenestrids became limited in their diffusive CO_2 uptake or other, fast-changing (a)biotic environmental factors limited the ecological success of this group. On million-year timescales, atmospheric CO_2 levels appear to have influenced coccolithophore macroevolution more than related long-term changes in temperature, sea level, ocean circulation or global carbon cycling (Hannisdal et al., 2012). Between biotic and abiotic factors, the latter

(i.e., nutrient supply, temperature, salinity, etc.) are deemed to be dominant (Benton, 2009) and may have led to a more successful adaptation of the smaller taxa at the expense of large ones (see discussion below, Sect. 5.2).

This would not exclude a transient, long-term $p\text{CO}_2$ forcing on coccolithophore evolution (Hannisdal et al., 2012). Interestingly, the decline in large *R. umbilicus* occurred earlier at Site 1263 (~33.8 Ma) than at higher latitudes in the Southern Ocean (~33.3 Ma at Site 689, Persico and Villa, 2004; ~33.5 Ma at Site 748, Villa et al., 2008). A similar pattern is documented in the timing of its subsequent extinction, occurring earlier at mid- and low latitudes (32.02 Ma; Pälike et al., 2006) and later at high latitudes (31.35 Ma; Gradstein et al., 2012). Henderiks and Pagani (2008) suggested that the generally higher content of CO_2 in polar waters may have sustained *R. umbilicus* populations after it had long disappeared from the tropics.

5.2 Paleoproductivity at Site 1263: nannoplankton and benthic foraminifer signals

At Site 1263, no other phytoplankton than calcareous nannoplankton was detected, and diatoms were absent in coeval sediments at nearby DSDP Walvis Ridge Sites 522–529 (Hsü et al., 1984; Moore et al., 1984). Therefore, our inferences of paleo-primary productivity and export production are based on the nannoplankton and benthic foraminiferal assemblages.

PC2 of the calcareous nannoplankton analysis could be correlated with paleoproductivity and total water column stratification. The strongest negative loading on PC2 is the holococcolith *L. minutus* (Fig. 4b; Table S1). In modern phytoplankton, the holococcolith-bearing life stages proliferate under oligotrophic conditions (e.g., Winter et al., 1994). Moreover, holococcoliths such as *L. minutus* and *Z. bijugatus* are quite robust (Dunkley Jones et al., 2008), so that dissolution is unlikely to affect their distribution.

The positive loadings on PC2 are the species *C. pelagicus*, *I. recurvus* and *Sphenolithus* spp. A high abundance of *C. pelagicus* has often been considered as indicative of warm to temperate temperatures at high latitudes (e.g., Wei and Wise, 1990; Persico and Villa, 2004; Villa et al., 2008). In the modern oceans, *C. pelagicus* seems to be restricted to temperate to cool water and high-nutrient conditions (e.g., Cachao and Moita, 2000; Boeckel et al., 2006), but during the Paleogene it was cosmopolitan (Haq and Lohmann, 1976). The paleoecological preferences of *Sphenolithus* are still controversial, but it has been related to oligotrophic conditions, inferring a major nutrient control rather than temperature control on this species during the Paleocene–Eocene thermal maximum (PETM; Agnini et al., 2006) and the EOT (Villa et al., 2008). Increased abundances of *Sphenolithus* have been also related to high-productivity intervals in the early Oligocene (Wade and Pälike, 2004) and across the EOT (Dunkley Jones et al., 2008).

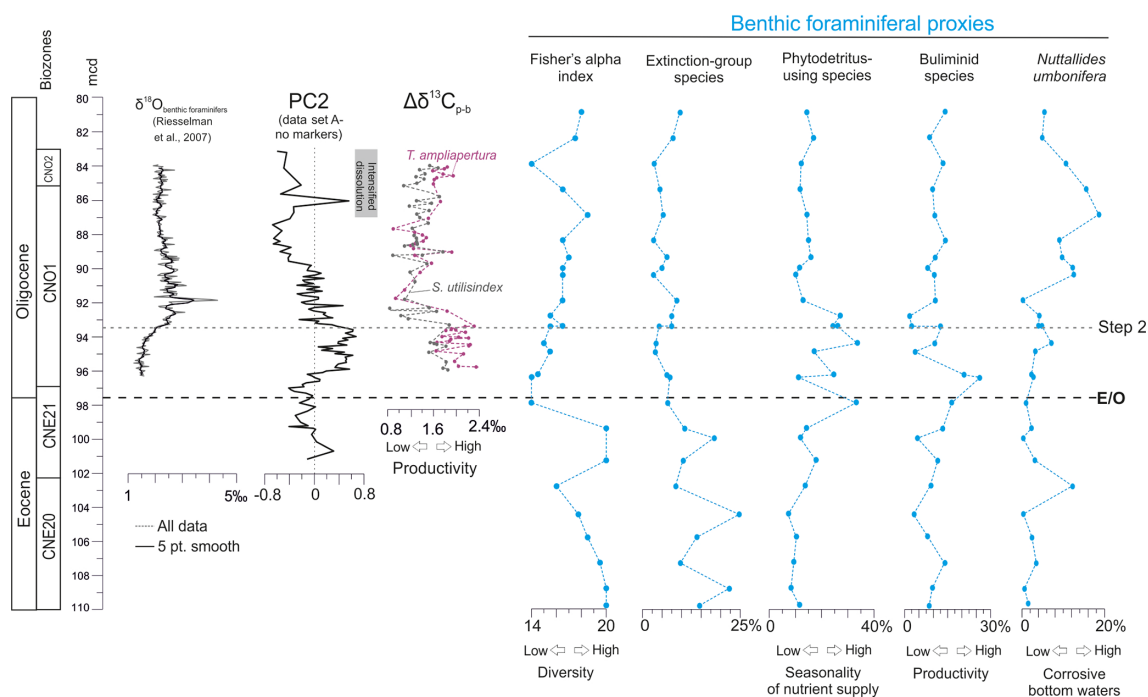


Figure 6. Paleoproductivity indices from nannofossil (PC2) and benthic foraminifer ($\Delta\delta^{13}\text{C}_{\text{P-B}}$ calculated from data in Riesselman et al. (2007) and Peck et al. (2010); Fisher's alpha index – diversity proxy, Extinction Group species, phytodetritus-using species, buliminid species and the species *Nuttallides umbonifera*) datums are plotted against depth. The positions of EOB and Step 2 are reported.

We compared PC2 with the proxy for regional paleoproductivity $\Delta\delta^{13}\text{C}_{\text{P-B}}$ (Fig. 6), with lower values corresponding to lower productivity, and/or higher stratification. $\Delta\delta^{13}\text{C}_{\text{P-B}}$ data are not available for the interval below 96 mcd (upper Eocene to lower Oligocene), but lower paleoproductivity in general corresponds to negative loadings on PC2 and vice versa. The correlation coefficient between the two curves is 0.33 (p value = 0.05), i.e., a significant but not very strong correlation, possibly due to the lower number of stable isotope data points than nannofossil data points. We infer that PC2 probably reflects lower productivity during the latest Eocene, with both PC2 and $\Delta\delta^{13}\text{C}_{\text{P-B}}$ curves showing higher productivity within the EOB and the onset of Step 2 (Fig. 6). In particular, PC2 records a longer interval of positive loadings (higher productivity) after the EOB and an initial decrease corresponding to the highest peak in $\delta^{18}\text{O}$ (at ~ 93 mcd; ~ 33.5 Ma), as recorded also by $\Delta\delta^{13}\text{C}_{\text{P-B}}$. According to the $\Delta\delta^{13}\text{C}_{\text{P-B}}$, paleoproductivity remained constant above 90 mcd upward, and lower than below Step 2. The different trend in PC2 from 90 mcd upward may be related to increased nannofossil dissolution, in particular above 87 mcd. The increase in dissolution is confirmed by the increased abundance of the benthic foraminifer species *N. umbonifera*, indicative of more corrosive bottom waters and the intensified dissolution interval recorded by the coccolith dissolution index (compare Figs. 3 and 6).

The benthic foraminiferal assemblage confirms the above interpretation of the PC2, adding information on the nature of the supply of organic matter to the seafloor, i.e., export productivity (Fig. 6). The increase in abundance of the phytodetritus-using species across the EOB indicates an increase in seasonality of food delivery to the seafloor, correlated to the interval with positive scores on PC2 (Fig. 6). The interval was interrupted by a short period of increased productivity across the EOB (as shown by the peak in the buliminid species curve at 96.27 mcd; Fig. 6), indicating high, less seasonally interrupted food supply. Seafloor conditions changed after Step 2, when the high abundance of *N. umbonifera* and the decrease in phytodetritus and buliminid species indicate more corrosive bottom waters, possibly combined with less food arriving at the sea floor and a less pronounced seasonality (Fig. 6).

Variations in nutrient supply to the photic zone, as reflected in nannofossils, represent a factor that could possibly have combined with the declining $p\text{CO}_2$ to cause the decrease in the mean coccolith size after the EOB. The transient higher availability of nutrients between the EOB and the onset of Step 2 (~ 330 kyr) may have given small opportunistic nannoplankton species a competitive advantage over large specialist species after this time. The decrease in mean cell size (less biomass per individual) and the overall decrease in nannofossil abundance could have led to less available organic matter or less efficient ballasting of organic

matter during transport to the sea floor and less food for the benthic foraminifers. If the smaller size led to decreased efficiency in ballasting, the time of transport from surface to the sea floor could have increased, making remineralization more efficient despite the declining temperatures. Ecosystem structure is the main determinant of efficiency of transfer of organic matter to the sea floor (e.g., Henson et al., 2012), and such important changes as observed in the nannofossil assemblages could have strongly impacted the transfer of food to the seafloor, and hence to benthic foraminiferal assemblages, and influenced the decline in Extinction Group species (Hayward et al., 2012; Mancin et al., 2013).

Possibly, climate-driven instability of the water column within 330 kyr after the EOB favored seasonal or episodic upwelling, and thus primary productivity in this area, which may also be reflected by the (slightly) increasing trends in the absolute abundance of (medium-sized) *Cyclicargolithus* spp., *C. pelagicus* and *Sphenolithus* spp. (Fig. 3). After the major peak in $\delta^{18}\text{O}$ (Step 2) a more stable system may have allowed the proliferation of more oligotrophic taxa, including holococcoliths, and the establishment of more oligotrophic, stable environmental conditions (Fig. 6).

Previous studies documented an increase in primary productivity during the late Eocene to early Oligocene, in particular in the Southern Ocean (e.g., Diester-Haass, 1995; Diester-Haass and Zahn, 1996; Salamy and Zachos, 1999; Persico and Villa, 2004; Schumacher and Lazarus, 2004; Anderson and Delaney, 2005). At tropical latitudes, both transient increases (equatorial Atlantic; Diester-Haass and Zachos, 2003) and decreases (e.g., Griffith et al., 2010; Moore et al., 2014) in paleoproductivity have been recorded during the early Oligocene, with a sharp drop in the export productivity during the early Oligocene at ~ 33.7 Ma (Moore et al., 2014), similar to what we observed in the SE Atlantic. Schumacher and Lazarus (2004) did not record a significant shift in paleoproductivity after the EOB in equatorial oceans but noted a decrease in the early Oligocene (after 31 Ma). An increase in seasonality after the EOB, similar to the one we recorded at midlatitudinal Site 1263, was documented at Site 689 in the Southern Ocean (Schumacher and Lazarus, 2004), while seasonality increased just before Step 2 at northern high latitudes (Eldrett et al., 2009).

5.3 Timing and possible causes of the biotic response at the EOB

Marine faunal and floral extinctions and community changes were coeval with the climatic deterioration during the late Eocene to early Oligocene (e.g., Adams et al., 1986; Cocconi, 1988; Berggren and Pearson, 2005; Dunkley Jones et al., 2008; Pearson et al., 2008; Tori, 2008; Villa et al., 2008, 2014). At ODP Site 1263, we see a close correspondence between marked changes in the nannoplankton assemblages (i.e., nannofossil abundance and coccolith size decrease) and the benthic foraminiferal assemblages. The nannoplankton

did not suffer extinctions at the EOB that were as significant as affecting the planktonic foraminiferal assemblage, but the change in the community was as fast as extinction events (which occur within 10–100 kyr; Gibbs et al., 2005; Raffi et al., 2006), taking place within ~ 47 kyr.

The main shifts in the nannoplanktonic community occurred during the EOT climatic transition, ~ 250 kyr after Step 1 and ~ 120 kyr after the EOB, but predated the major cooling and increase in Antarctic ice sheet volume (i.e., Step 2) by about 200 kyr. Therefore, nannofossil assemblages prove to be sensitive and accurate tools to investigate climate thresholds and the early impacts of climate change on biotic systems.

Benthic foraminiferal changes at Site 1263 started before the EOB, as observed at other sites (Thomas, 1990, 2007), and the faunal turnover persisted into the early Oligocene. The benthic faunas in general show a decline in abundance of rectilinear species with complex apertures, possibly linked to the decline in nannoplankton species which they may have consumed (as, e.g., hypothesized by Hayward et al., 2012; Mancin et al., 2013). The increase in phytodetritus-using species was possibly linked to more episodic upwelling and thus productivity and transport to the sea floor and potentially the blooming of more opportunistic nannoplankton species. Unfortunately, the lower resolution of the benthic foraminifer data compared to the nannofossil data does not allow us to unravel the exact timing of the benthic fauna response during the EOT and also does not allow the exact correlation with changes in nannofossil assemblages.

At Site 1263 and in Southern Ocean records (Persico and Villa, 2004; Villa et al., 2008), the large reticulofenestrads declined in abundance rapidly after the EOB. Persico and Villa (2004) and Villa et al. (2008, 2014) inferred a strong influence of SST cooling on coccolithophores, and the drop in SST shortly after the EOB at high latitudes is confirmed by a decrease in 5°C in $U_{37}^{K'}$ -based SST (Liu et al., 2009). In contrast, at Site 1263 planktonic foraminifer Mg/Ca data record no significant change in SST at that time (Peck et al., 2010; Fig. 5), as at ODP Sites 925 and 929 (tropical western Atlantic) where $U_{37}^{K'}$ -based SSTs show no significant cooling (Liu et al., 2009; Fig. 5). Fairly stable SSTs were also documented in the tropics, using Mg/Ca-based SST reconstructions (Lear et al., 2008). The temperatures at midlatitudinal Site 1263 thus may have been stable, like those in the tropics, rather than cooling, as inferred for high latitudes in the Southern Ocean (e.g., Persico and Villa, 2004; Villa et al., 2008; Liu et al., 2009; Villa et al., 2014).

If this is true, SST may not have been the main environmental factor affecting the nannoplankton assemblages at Site 1263 after the EOB. Andruleit et al. (2003) documented that temperature changes may be of less importance for modern coccolithophores in tropical and subtropical regions, but the lower temperature at high latitudes can approach the vital limits for coccolithophores (Baumann et al., 1997) and become important as a bio-limiting factor.

Changes in the phytoplankton community could be related to a global influence of declining $p\text{CO}_2$. Unfortunately the estimates from alkenone and boron isotopes lack the resolution to unravel the variation across and after the EOB (Fig. 5) in detail and leave open the possibility that $p\text{CO}_2$ falling below a certain threshold level could have played a role in driving the reorganization in the nannoplankton community. Alternatively, our combined biotic and geochemical proxy data (i.e., nannofossil and benthic foraminiferal assemblages and $\Delta\delta^{13}\text{C}_{\text{P-B}}$) suggest an increase in nutrient and food supply just after the EOB (Fig. 6), which would have favored opportunistic taxa over low-nutrient selected, specialist species. Most large reticulofenestrids (except *R. hillae* and *R. circus* group) never recovered to the level of previous abundances, despite a return to more stratified conditions after Step 2. It is unlikely that increased dissolution above 87 mcd (33 Ma) explains the loss of large, heavily calcified taxa, but the decrease in size of coccoliths may also have led to enhanced remineralization of organic matter and less food supply to the benthic communities.

There appears to be a latitudinal gradient in the timing of nannofossil abundance decreases. The total abundance decreases were first detected in the Southern Ocean (late Eocene; Persico and Villa, 2004), then at midlatitude (after the EOB; this study), and finally at the equator (after Step 2, as inferred from a decrease in nannofossil species diversity at Tanzanian sites; Dunkley Jones et al., 2008). This observation may suggest a direct temperature effect on nannoplankton abundance since nannofossil floras reflect the pattern of cooling, which started and was most pronounced at high latitudes. On the other hand, high-latitude cooling may have impacted the global nutrient regimes and ocean circulation. Since regional dissolution bias may also have affected the comparison of absolute coccolith abundance, additional studies on well-preserved material will be necessary to confirm the timing and character of the response at different latitudes and in different ocean basins. Nevertheless, a meridional gradient in biotic response is expected, given the different environmental sensitivities and biogeographic ranges of different phytoplankton species (e.g., Wei and Wise, 1990; Monechi et al., 2000; Persico and Villa, 2004; Villa et al., 2008) and the diachroneity of the onset of cooling (Pearson et al., 2008).

6 Conclusions

High-resolution analyses of the calcareous nannofossil and foraminiferal assemblages refine the biostratigraphy at ODP Site 1263 (Walvis Ridge) and demonstrate distinct assemblage and abundance changes in marine biota across the Eocene–Oligocene transition. The biotic response of calcareous nannoplankton was very rapid (~ 47 kyr), following the EOB by ~ 120 kyr and predating the climatic Step 2 event by 200 kyr.

The ecological success of smaller-sized coccolithophore species vs. the drastic decrease in large reticulofenestrids, and the overall decrease in nannoplankton productivity after the EOB likely affected the benthic foraminiferal community (e.g., decrease in rectilinear species due to changes in nannoplankton floras), with increased seasonality driving the transient increased abundance of phytodetritus-using species. After Step 2 and in particular after 33.3 Ma, both nannoplankton and benthic records at Site 1263 were affected by intensified dissolution and corrosivity of bottom waters.

We conclude that the planktonic community reacted to fast-changing environmental conditions – possibly seasonally increased nutrient supply to the photic zone, global cooling or lowered CO_2 availability – and/or the crossing of a threshold level in the longer-term climate and environmental changes suggested by available proxy data, such as the transient $p\text{CO}_2$ decline during the late Eocene to early Oligocene.

The Supplement related to this article is available online at doi:10.5194/cp-11-1249-2015-supplement.

Acknowledgements. The authors are grateful to the International Ocean Discovery Program (IODP) core repository in Bremen for providing samples for this research. The ODP (now IODP) was sponsored by the US National Science Foundation and participating countries under management of the Joint Oceanographic Institutions (JOI), Inc. We are thankful to Tom Dunkley Jones, Giuliana Villa and an anonymous reviewer for their constructive suggestions. We also thank Paul Pearson for his helpful comments. The project was financially supported by the Swedish Research Council (VR grant 2011-4866 to J. Henderiks), by MIUR-PRIN grant 2010X3PP8J 005 (to S. Monechi), and by Spanish Ministry of Science and Technology (FEDER funds) Project CGL2011-23077 (grant BES-2012-058945 to A. Legarda-Lisarrri). E. Thomas acknowledges the Geological Society of America and the Leverhulme Foundation (UK) for research support. We are grateful to Davide Persico and Nicolàs Campione for discussions on the statistical approach and to Helen Coxall for helpful suggestions on the oxygen isotope stratigraphy.

Edited by: G. Dickens

References

- Adams, C. G., Butterlin, J., and Samanta, B. K.: Larger foraminifera and events at the Eocene–Oligocene boundary in the Indo–West Pacific region, in: Terminal Eocene Events, edited by: Pomeroy, C. and Premoli Silva, I., Elsevier, Amsterdam, 237–252, 1986.
- Adler, M., Hensen, C., Wenzhöfer, F., Pfeifer, K., and Schulz, H. D.: Modelling of calcite dissolution by oxic respiration in supralysoclineal deep-sea sediments, *Mar. Geol.*, 177, 167–189, 2001.

- Agnini, C., Fornaciari, E., Rio, D., Tateo, F., Backman, J., and Giusberti, L.: Responses of calcareous nannofossil assemblages, mineralogy and geochemistry to the environmental perturbations across the Paleocene Eocene boundary in the Venetian Pre-Alps, *Mar. Micropaleontol.*, 63, 19–38, 2006.
- Agnini, C., Fornaciari, E., Raffi, I., Catanzariti, R., Pälke, H., Backman, J., and Rio, D.: Biozonation and biochronology of Paleogene calcareous nannofossils from low and middle latitudes, *Newsletters on Stratigraphy*, 47, 131–181, 2014.
- Aitchison, J.: The statistical analysis of compositional data. Chapman and Hall, London, 416 pp., 1986.
- Anderson, L. D. and Delaney, L. M.: Middle Eocene to early Oligocene paleoceanography from the Agulhas Ridge, Southern Ocean (Ocean Drilling Program Leg 177, Site 1090), *Paleoceanography*, 20, PA1013, doi:10.1029/2004PA001043, 2005.
- Andruleit, H., Stäger, S., Rogalla, U., and Čeppek, P.: Living coccolithophores in the northern Arabian Sea: ecological tolerances and environmental control, *Mar. Micropaleontol.*, 49, 157–181, 2003.
- Aubry, M.-P.: Late Paleogene calcareous nannoplankton evolution; a tale of climatic deterioration, in: *Eocene-Oligocene Climatic and Biotic Evolution*, edited by: Prothero, D. R. and Berggren, W. A., Princeton University Press, 272–309, 1992.
- Auer, G., Piller, W. E., and Harzhauser, M.: High-resolution calcareous nannoplankton palaeoecology as a proxy for small-scale environmental changes in the Early Miocene, *Mar. Micropaleontol.*, 111, 53–65, 2014.
- Backman, J.: Quantitative calcareous nannofossil biochronology of middle Eocene through early Oligocene sediment from DSDP Sites 522 and 523, *Abhandlungen der Geologischen Bundesanstalt*, Vienna, 39, 21–31, 1987.
- Barker, P. F. and Thomas, E.: Origin, signature and palaeoclimatic influence of the Antarctic Circumpolar Current, *Earth Science Reviews*, 66, 143–162, 2004.
- Baumann, K.-H., Andruleit, H., Schröder-Ritzrau, A., and Samtleben, C.: Spatial and temporal dynamics of coccolithophore communities during non-production phases in the Norwegian-Greenland Sea, in: *Contributions to the Micropaleontology and Paleoceanography of the Northern North Atlantic*, edited by: Hass, H. C. and Kaminski, M. A., Grzybowski Foundation Special Publication, 5, 227–243, 1997.
- Beaufort, L., Probert, I., and Buchet, N.: Effects of acidification and primary production on coccolith weight: Implications for carbonate transfer from the surface to the deep ocean, *Geochem. Geophys. Geosy.*, 8, 1–18, 2007.
- Benson, R. H.: The origin of the psychrosphere as recorded in changes of deep-sea ostracode assemblages, *Lethaia*, 8, 69–83, 1975.
- Benton, M. J.: The Red Queen and the Court Jester: species diversity and the role of biotic and abiotic factors through time, *Science*, 323, 728–732, 2009.
- Berger, W. H.: Deep-sea carbonates: evidence for a coccolith lysocline, *Deep-Sea Research and Oceanographic Abstracts*, 20, 917–921, 1973.
- Berggren, W. A. and Pearson, P. N.: A revised tropical to subtropical Paleogene planktonic foraminifera zonation, *J. Foramin. Res.*, 35, 279–298, 2005.
- Berggren, W. A., Kent, D. V., Swisher, C. C., and Aubry, M.-P.: A revised Cenozoic geochronology and chronostratigraphy, in: *Geochronology, time scales and global stratigraphic correlation*, *SEPM Spec. Publ.*, 54, 129–212, 1995.
- Blaj, T., Backman, J., and Raffi, I.: Late Eocene to Oligocene preservation history and biochronology of calcareous nannofossils from paleo-equatorial Pacific Ocean sediments, *Riv. Ital. Paleontol. S.*, 115, 67–85, 2009.
- Boeckel, B., Baumann, K.-H., Henrich, R., and Kinkel, H.: Coccolith distribution patterns in South Atlantic and Southern Ocean surface sediments in relation to environmental gradients, *Deep-Sea Res. Pt. I*, 53, 1073–1099, 2006.
- Bohaty, S. M., Zachos, J. C., and Delaney, M. L.: Foraminiferal Mg/Ca evidence for Southern Ocean cooling across the Eocene/Oligocene transition, *Earth Planet. Sc. Lett.*, 317, 251–261, 2012.
- Bollmann, J., Bräbec, B., Cortes, M., and Geisen, M.: Determination of absolute coccolith abundances in deep-sea sediments by spiking with microbeads and spraying (SMS method), *Mar. Micropaleontol.*, 38, 29–38, 1999.
- Bolton, C. T. and Stoll, H.: Late Miocene threshold response of marine algae to carbon dioxide limitation, *Nature*, 500, 558–562, 2013.
- Bordiga, M., Beaufort, L., Cobianchi, M., Lupi, C., Mancin, N., Luciani, V., Pelosi, N., and Sprovieri, M.: Calcareous plankton and geochemistry from the ODP site 1209B in the NW Pacific Ocean (Shatsky Rise): new data to interpret calcite dissolution and paleoproductivity changes of the last 450 ka, *Palaeogeogr. Palaeoclimatol.*, 371, 93–108, 2013.
- Bordiga, M., Bartol, M., and Henderiks, J.: Absolute nannofossil abundance estimates: Quantifying the pros and cons of different techniques, *Revue de micropaléontologie*, 155–165, doi:10.1016/j.revmic.2015.05.002, 2015.
- Boscolo-Galazzo, F., Thomas, E., and Giusberti, L.: Benthic foraminiferal response to the Middle Eocene Climatic Optimum (MECO) in the South-Eastern Atlantic (ODP Site 1263), *Palaeogeogr. Palaeoclimatol.*, 417, 432–444, 2015.
- Bown, P. R. and Dunkley Jones, T.: New Paleogene calcareous nannofossil taxa from coastal Tanzania: Tanzania Drilling Project Sites 11 to 14, *J. Nannoplankton Res.*, 28, 17–34, 2006.
- Bown, P. R. and Young, J. R.: Techniques, in: *Calcareous Nannofossil Biostratigraphy*, edited by: Bown, P. R., Chapman and Hall, Cambridge, 16–28, 1998.
- Bown, P. R., Lees, J. A., and Young, J. R.: Calcareous nannoplankton evolution and diversity through time, in: *Coccolithophores*, edited by: Thierstein, H., R. and Young J. R., Springer Berlin Heidelberg, 481–508, 2004.
- Bown, P. R., Dunkley Jones, T., Lees, J. A., Randell, R. D., Mizzi, J. A., Pearson, P. N., Coxall, H. K., Young, J. R., Nicholas, C. J., Karega, A., Singano, J., and Wade, B. S.: A Paleogene calcareous microfossil Konservat-Lagerstätte from the Kilwa Group of coastal Tanzania, *Geol. Soc. Am. Bull.*, 120, 3–12, 2008.
- Bremer, M. L. and Lohmann, G. P.: Evidence for primary control of the distribution of certain Atlantic Ocean benthonic foraminifera by degree of carbonate saturation, *Deep-Sea Res.*, 29, 987–998, 1982.
- Buccianti, A. and Esposito, P.: Insights into Late Quaternary calcareous nannoplankton assemblages under the theory of statistical analysis for compositional data, *Palaeogeogr. Palaeoclimatol.*, 202, 209–277, 2004.

- Cachao, M. and Moita, M. T.: *Coccolithus pelagicus*, a productivity proxy related to moderate fronts off Western Iberia, *Mar. Micropaleontol.*, 39, 131–155, 2000.
- Coccioni, R.: The genera *Hantkenina* and *Cribohantkenina* (foraminifera) in the Massignano section (Ancona, Italy), in: *The Eocene–Oligocene boundary in the Marche–Umbria basin (Italy)*, edited by: Premoli Silva, I., Coccioni, R., and Montanari, A., International Subcommission on the Paleogene Stratigraphy, Eocene Oligocene Meeting, Ancona, Spec. Publ., 2, 81–96, 1988.
- Coxall, H. K. and Pearson, P. N.: Taxonomy, biostratigraphy, and phylogeny of the Hantkeninidae (*Clavigerinella*, *Hantkenina*, and *Cribohantkenina*), in: *Atlas of Eocene Planktonic Foraminifera*, edited by: Pearson, P. N., Olsson, R. K., Huber, B. T., Hemleben, C., and Berggren, W. A., Cushman Foundation Special Publication, 41, 216–256, 2006.
- Coxall, H. K. and Pearson, P. N.: The Eocene–Oligocene transition, in: *Deep-time perspectives on climate change: marrying the signal from computer models and biological proxies*, edited by: Williams, M., Haywood, A. M., Gregory, F. J., and Schmidt, D. N., Geological Society (London), Micropaleontological Society, 351–387, 2007.
- Coxall, H. K. and Wilson, P. A.: Early Oligocene glaciation and productivity in the eastern equatorial Pacific: insights into global carbon cycling, *Paleoceanography*, 26, PA2221, doi:10.1029/2010PA002021, 2011.
- Coxall, H. K., Wilson, P. A., Pälike, H., Lear, C. H., and Backman, J.: Rapid stepwise onset of Antarctic glaciation and deeper calcite compensation in the Pacific Ocean, *Nature*, 433, 53–57, 2005.
- Daniels, C. J., Sheward, R. M., and Poulton, A. J.: Biogeochemical implications of comparative growth rates of *Emiliania huxleyi* and *Coccolithus* species, *Biogeosciences*, 11, 6915–6925, doi:10.5194/bg-11-6915-2014, 2014.
- De Kaenel, E. and Villa, G.: Oligocene–Miocene calcareous nannofossil biostratigraphy and paleoecology from the Iberia abyssal plain, in: *Proceedings ODP, Scientific Results, College Station, TX (Ocean Drilling Program)*, 149, 79–145, 1996.
- DeConto, R. M. and Pollard, D.: Rapid Cenozoic glaciation of Antarctica induced by declining atmospheric CO₂, *Nature*, 421, 245–249, 2003.
- De Villiers, S.: Foraminiferal shell-weight evidence for sedimentary calcite dissolution above the lysocline, *Deep-Sea Res. Pt. I*, 52, 671–680, 2005.
- Diester-Haass, L.: Middle Eocene to early Oligocene paleoceanography of the Antarctic Ocean (Maud Rise, ODP Leg 113, Site 689): change from low productivity to a high productivity ocean, *Palaeogeogr. Palaeoclimatol.*, 113, 311–334, 1995.
- Diester-Haass, L. and Zachos, J. C.: The Eocene–Oligocene transition in the Equatorial Atlantic (ODP Site 325), paleoproductivity increase and positive $\delta^{13}\text{C}$ excursion, in: *from greenhouse to icehouse: the marine Eocene–Oligocene transition*, edited by: Prothero, D. R., Ivany, L. C., and Nesbitt, E. A., Columbia University Press, New York, 397–416, 2003.
- Diester-Haass, L. and Zahn, R.: Eocene–Oligocene transition in the Southern Ocean: history of water mass circulation and biological productivity, *Geology*, 24, 163–166, 1996.
- Dockery III, D. T.: Punctuated succession of marine mollusks in the northern Gulf Coastal Plain, *Palaos*, 1, 582–589, 1986.
- Dunkley Jones, T., Bown, P. R., Pearson, P. N., Wade, B. S., Coxall, H. K., and Lear, C. H.: Major shift in calcareous phytoplankton assemblages through the Eocene–Oligocene transition of Tanzania and their implications for low-latitude primary production, *Paleoceanography*, 23, PA4204, doi:10.1029/2008PA001640, 2008.
- Eldrett, J. S., Greenwood, D. R., Harding, I. C., and Hubber, M.: Increased seasonality through the Eocene to Oligocene transition in northern high latitudes, *Nature*, 459, 969–973, 2009.
- Falkowski, P. G., Katz, M. E., Knoll, A. H., Quigg, A., Raven, J. A., Schofield, O., and Tayler, F. J. R.: The evolution of modern eukaryotic plankton, *Science*, 305, 354–360, 2004.
- Fenero, R., Thomas, E., Alegret, L., and Molina, E.: Evolución paleoambiental del tránsito Eoceno–Oligoceno en el Atlántico sur (Sondeo 1263) basada en foraminíferos bentónicos, *Geogaceta*, 49, 3–6, 2010 (in Spanish).
- Fioroni, C., Villa, G., Persico, D., and Jovane, L.: Middle Eocene–Lower Oligocene calcareous nannofossil biostratigraphy and paleoceanographic implications from Site 711 (equatorial Indian Ocean), *Mar. Micropaleontol.*, 118, 50–62, 2015.
- Foster, L. C., Schmidt, D. N., Thomas, E., Arndt, S., and Ridgwell, A.: Surviving rapid climate change in the deep sea during the Paleogene hyperthermals, *P. Natl. Acad. Sci.*, 110, 9273–9276, 2013.
- Geisen, M., Bollmann, J., Herrle, J. O., Mutterlose, J., and Young, J. R.: Calibration of the random settling technique for calculation of absolute abundances of calcareous nannoplankton, *Micropaleontology*, 45, 437–442, 1999.
- Gibbs, S. J., Shackleton, N. J., and Young, J. R.: Identification of dissolution patterns in nannofossil assemblages: a high-resolution comparison of synchronous records from Ceara Rise, ODP Leg 154, *Paleoceanography*, 19, PA1029, doi:10.1029/2003PA000958, 2004.
- Gibbs, S. J., Young, J. R., Bralower, T. J., and Shackleton, N. J.: Nannofossil evolutionary events in the mid-Pliocene: an assessment of the degree of synchrony in the extinctions of *Reticulofenestra pseudumbilicus* and *Sphenolithus abies*, *Palaeogeogr. Palaeoclimatol.*, 217, 155–172, 2005.
- Gibbs, S. J., Bown, P. R., Murphy, B. H., Sluijs, A., Edgar, K. M., Pälike, H., Bolton, C. T., and Zachos, J. C.: Interactive comment on “Scaled biotic disruption during early Eocene global warming events”, *Biogeosciences Discuss.*, 9, C618–C620, www.biogeosciences-discuss.net/9/C618/2012/, 2012.
- Giordano, M., Beardall, J., and Raven, A.: CO₂ concentrating mechanisms in algae: mechanisms, environmental modulation, and evolution, *Annu. Rev. Plant. Biol.*, 56, 99–131, 2005.
- Goldner, A., Herold, N., and Huber, M.: Antarctic glaciation caused ocean circulation changes at the Eocene–Oligocene transition, *Nature*, 511, 574–578, 2014.
- Gooday, A. J.: Benthic foraminifera (Protista) as tools in deep-water paleoceanography: environmental influences on faunal characteristics, *Adv. Mar. Biol.*, 46, 1–90, 2003.
- Gooday, A. J. and Jorissen, F. J.: Benthic foraminiferal biogeography: controls on global distribution patterns in deep-water settings, *Annu. Rev. Mar. Sci.*, 4, 237–262, 2012.
- Gradstein, F. M., Ogg, J. G., Schmitz, M., and Ogg, G.: *The Geologic Time Scale 2012*, Vol. 2, Elsevier, 1144 pp., 2012.
- Griffith, E., Calhoun, M., Thomas, E., Averyt, K., Erhardt, A., Bralower, T., Lyle, M., Olivarez-Lyle, A., and Paytan, A.: Ex-

- port productivity and carbonate accumulation in the Pacific Basin at the transition from greenhouse to icehouse climate (Late Eocene to Early Oligocene), *Paleoceanography*, 25, PA3212, doi:10.1029/2010PA001932, 2010.
- Hammer, Ø. and Harper, D. A. T.: Paleontological data analysis, Blackwell, Malden, USA, 370 pp., 2006.
- Hammer, Ø., Harper, D. A. T., and Ryan, P. D.: PAST: Paleontological Statistics Software Package for education and data analysis, *Palaeontologia Electronica*, 4, 1–9, http://palaeo-electronica.org/2001_2001/past/issue2001_2001.htm, 2001.
- Hannisdal, B., Henderiks, J., and Liow, L. H.: Long-term evolutionary and ecological responses of calcifying phytoplankton to changes in atmospheric CO₂, *Glob. Change Biol.*, 18, 3504–3516, 2012.
- Haq, B. U. and Lohmann, G. P.: Early Cenozoic calcareous nannoplankton biogeography of the Atlantic Ocean, *Mar. Micropaleontol.*, 1, 119–194, 1976.
- Hayek, L.-A. C. and Buzas, M. A.: Surveying natural populations: quantitative tools for assessing biodiversity, Columbia University Press, 590 pp., 2010.
- Hayward, B. W., Kawagata, S., Sabaa, A. T., Grenfell, H. R., van Kerckhoven, L., Johnson, K., and Thomas, E.: The last global extinction (Mid-Pleistocene) of deep-sea benthic foraminifera (Chrysalogoniidae, Ellipsoidinidae, Glandulonodosariidae, Plectofrondiculariidae, Pleurostomellidae, Stilostomellidae), their Late Cretaceous–Cenozoic history and taxonomy. Cushman Foundation For Foraminiferal Research, Spec. Publ., 43, 408 pp., 2012.
- Henderiks, J.: Coccolithophore size rules – reconstructing ancient cell geometry and cellular calcite quota from fossil coccoliths, *Mar. Micropaleontol.*, 67, 143–154, 2008.
- Henderiks, J. and Pagani, M.: Refining ancient carbon dioxide estimates: significance of coccolithophore cell size for alkenone-based pCO₂ records, *Paleoceanography*, 22, PA3202, doi:10.1029/2006PA001399, 2007.
- Henderiks, J. and Pagani, M.: Coccolithophore cell size and Paleogene decline in atmospheric CO₂, *Earth Planet. Sc. Lett.*, 269, 576–584, 2008.
- Henderiks, J., Winter, A., Elbrächter, M., Feistel, R., van der Plas, A. K., Nausch, G., and Barlow, R.: Environmental controls on *Emiliania huxleyi* morphotypes in the Benguela coastal upwelling system (SE Atlantic), *Mar. Ecol.-Prog. Ser.*, 448, 51–66, 2012.
- Henson, S. A., Sanders, R., and Madsen, E.: Global patterns in efficiency of particulate organic carbon export and transfer to the deep ocean, *Global Biogeochem. Cy.*, 26, GB1028, doi:10.1029/2011GB004099, 2012.
- Hsü, K. J., LaBrecque, J. L., Carman Jr., M. F., and Shipboard Scientific Party: Site 522, in: DSDP, Initial Reports, College Station, TX, 73, 187–270, 1984.
- Hyland, E., Murphy, B., Varela, P., Marks, K., Colwell, L., Tori, F., Monechi, S., Cleaveland, L., Brinkhuis, H., Van Mourik, C. A., Coccioni, R., Bice, D., and Montanari, A.: Integrated stratigraphic and astrochronologic calibration of the Eocene–Oligocene transition in the Monte Cagnero section (northeastern Apennines, Italy): a potential parastratotype for the Massignano global stratotype section and point (GSSP), in: *The Late Eocene Earth: Hothouse, Icehouse, and Impacts*, edited by: Koeberl, C. and Montanari, A., *Geol. S. Am. S.*, 452, 303–322, 2009.
- Jennions, S. M., Thomas, E., Schimdt, D. N., Lunt, D., and Ridgwell, A.: Changes in benthic ecosystems and ocean circulation in the Southeast Atlantic across Eocene Thermal Maximum 2, *Paleoceanography*, 30, 1059–1077, doi:10.1002/2015PA002821, 2015.
- Jorissen, F. J., de Stigter, H. C., and Widmark, J. G. V.: A conceptual model explaining benthic foraminiferal microhabitats, *Mar. Micropaleontol.*, 26, 3–15, 1995.
- Jorissen, F. J., Fontanier, C., and Thomas, E.: Paleooceanographical proxies based on deep-sea benthic foraminiferal assemblage characteristics, in: *Proxies in Late Cenozoic Paleooceanography: Pt. 2: Biological tracers and biomarkers*, edited by: Hillaire-Marcel, C. and de Vernal, A., Elsevier, 263–326, 2007.
- Katz, M. E., Miller, K. G., Wright, J. D., Wade, B. S., Browning, J. V., Cramer, B. S., and Rosenthal, Y.: Stepwise transition from the Eocene greenhouse to the Oligocene icehouse, *Nat. Geosci.*, 1, 329–334, 2008.
- Keller, G.: Stepwise mass extinctions and impact events: Late Eocene to early Oligocene, *Mar. Micropaleontol.*, 10, 267–293, 1986.
- Kennett, J. P.: Cenozoic evolution of Antarctic glaciation, the circum-Antarctic Ocean, and their impact on global paleoceanography, *J. Geophys. Res.*, 82, 3843–3860, 1977.
- Koch, C. and Young, J. R.: A simple weighing and dilution technique for determining absolute abundances of coccoliths from sediment samples, *J. Nanoplankt. Res.*, 29, 67–69, 2007.
- Kucera, M. and Malmgren, B. A.: Logratio transformation of compositional data – a resolution of the constant sum constraint, *Mar. Micropaleontol.*, 34, 117–120, 1998.
- Ladant, J.-B., Donnadieu, Y., and Dumas, C.: Links between CO₂, glaciation and water flow: reconciling the Cenozoic history of the Antarctic Circumpolar Current, *Clim. Past*, 10, 1957–1966, doi:10.5194/cp-10-1957-2014, 2014.
- Lear, C. H., Bailey, T. R., Pearson, P. N., Coxall, H. K., and Rosenthal, Y.: Cooling and ice growth across the Eocene–Oligocene transition, *Geology*, 36, 251–254, 2008.
- Liu, Z., Tuo, S., Zhao, Q., Cheng, X., and Huang, W.: Deep-water earliest Oligocene Glacial Maximum (EOGM) in South Atlantic, *Chinese Sci. Bull.*, 49, 2190–2197, 2004.
- Liu, Z., Pagani, M., Zinniker, D., DeConto, R. M., Huber, M., Brinkhuis, H., Shah, S. R., Leckie, R. M., and Pearson, A.: Global cooling during the Eocene–Oligocene climate transition, *Science*, 323, 1187–1190, 2009.
- Lyle, M., Wilson, P. A., Janecek, T. R., and Shipboard Scientific Party: Leg 199 Summary, in: *Proceedings ODP, Initial Reports*, College Station, TX (Ocean Drilling Program), 199, 1–87, 2002.
- MacArthur, R. H.: On the relative abundance of species, *Am. Nat.*, 94, 25–36, 1960.
- Maiorano, P., Tarantino, F., Marino, M., and De Lange, G. J.: Paleoenvironmental conditions at Core KC01B (Ionina Sea) through MIS 13–9: evidence from calcareous nannofossil assemblages, *Quatern. Int.*, 288, 97–111, 2013.
- Mancin, N., Hayward, B. H., Trattenero, I., Cobianchi, M., and Lupi, C.: Can the morphology of deep-sea benthic foraminifera reveal what caused their extinction during the mid-Pleistocene Climate Transition?, *Mar. Micropaleontol.*, 104, 53–70, 2013.
- Marino, M. and Flores, J. A.: Middle Eocene to early Oligocene calcareous nannofossil stratigraphy at Leg 177 Site 1090, *Mar. Micropaleontol.*, 45, 291–307, 2002.

- Maronna, R., Martin, R. D., and Yohai, V. J.: Robust statistics: Theory and methods, Wiley J., New York, 436 pp., 2006.
- Martini, E.: Standard Tertiary and Quaternary calcareous nannoplankton zonation, Proc. 2nd Conf. Planktonic Microfossils, Rome, 2, 739–786, 1971.
- Meng, J. and McKenna, M. C.: Faunal turnovers of Palaeogene mammals from the Mongolian Plateau, *Nature*, 394, 364–367, 1998.
- Merico, A., Tyrrell, T., and Wilson, P. A.: Eocene/Oligocene ocean de-acidification linked to Antarctic glaciation by sea-level fall, *Nature* 452, 979–982, 2008.
- Miller, K. G., Wright, J. D., Katz, M. E., Wade, B. S., Browning, J. V., Cramer, B. S., and Rosenthal, Y.: Climate threshold at the Eocene-Oligocene transition: Antarctic ice sheet influence on ocean circulation, *Geol. Soc. Am. Spec. Pap.*, 452, 169–178, 2009.
- Milliman, J. D., Troy, P. J., Balch, W. M., Adams, A. K., Li, Y.-H., and Mackenzie, F. T.: Biologically mediated dissolution of calcium carbonate above the chemical lysocline? *Deep-Sea Res. Pt. I*, 46, 1653–1669, 1999.
- Mix, A. C., Morey, A. E., Pisias, N. G., and Hostetler, S. W.: Foraminiferal faunal estimates of paleotemperature: circumventing the no-analog problem yields cool ice age tropics, *Paleoceanography*, 14, 350–359, doi:10.1029/1999PA900012, 1999.
- Monechi, S., Buccianti, A., and Gardin, S.: Biotic signals from nanoflora across the iridium anomaly in the upper Eocene of the Massignano section: evidence from statistical analysis, *Mar. Micropaleontol.*, 39, 219–237, 2000.
- Moolna, A. and Rickaby, R. E. M.: Interaction of the coccolithophore *Gephyrocapsa oceanica* with its carbon environment: response to a recreated high-CO₂ geological past, *Geobiology*, 10, 72–81, 2012.
- Moore, T. C., Rabinowitz, P. D., and Shipboard Scientific Party: Site 525–529, in: Deep Sea Drilling Project, Initial Reports, US Government Printing Office, Washington, DC, USA, 74, 41–465, 1984.
- Moore, T. C., Wade, B. S., Westerhold, T., Erhardt, A., M., Coxall, H. K., Baldauf, J., and Wagner, M.: Equatorial Pacific productivity changes near the Eocene-Oligocene boundary, *Paleoceanography*, 29, 825–844, doi:10.1002/2014PA002656, 2014.
- Norris, R. D., Wilson, P. A., Blum, P., and the Expedition 342 Scientists: Proceedings IODP, 342, College Station, TX (Integrated Ocean Drilling Program), doi:10.2204/iodp.proc.342.2014, 2014.
- Ocean Drilling Stratigraphic Network, Plate Tectonic Reconstruction Service: <http://www.odsn.de/odsn/services/paleomap/paleomap.html> (last access: 10 April 2015), 2011.
- Ortiz, S. and Thomas, E.: Deep-sea benthic foraminiferal turnover during the early middle Eocene transition at Walvis Ridge (SE Atlantic), *Palaeogeogr. Palaeoclimatol.*, 417, 126–136, 2015.
- Pagani, M., Huber, M., Liu, Z., Bohaty, S. M., Henderiks, J., Sijp, W., Krishnan, S., and DeConto, R. M.: The role of carbon dioxide during the onset of Antarctic glaciation, *Science*, 334, 1261–1264, 2011.
- Pälike, H., Norris, R. D., Herrle, J. O., Wilson, P. A., Coxall, H. K., Lear, C. H., Shackleton, N. J., Tripathi, A. K., and Wade, B. S.: The heartbeat of the Oligocene climate system, *Science*, 314, 1894–1898, 2006.
- Pea, L.: Eocene-Oligocene paleoceanography of the subantarctic South Atlantic: calcareous nannofossil reconstructions of temperature, nutrient, and dissolution history, Ph.D. thesis, Department of Earth Sciences, University of Parma, Italy, 210 pp., 2010.
- Pearson, K.: Mathematical contributions to the theory of evolution. On a form of spurious correlation which may arise when indices are used in the measurement of organisms, *P. R. Soc. London*, 60, 489–498, 1896.
- Pearson, P. N., van Drogen, B. E., Nicholas, C. J., Pancost, R. D., Schouten, S., Singano, J. M., and Wade, B. S.: Stable warm tropical climate through the Eocene Epoch, *Geology*, 35, 211–214, 2007.
- Pearson, P. N., McMillan, I. K., Wade, B. S., Dunkley Jones, T., Coxall, H. K., Bown, P. R., and Lear, C. H.: Extinction and environmental change across the Eocene-Oligocene boundary in Tanzania, *Geology*, 36, 179–182, 2008.
- Pearson, P. N., Gavin, L. F., and Wade, B. S.: Atmospheric carbon dioxide through the Eocene–Oligocene climate transition, *Nature*, 461, 1110–1114, 2009.
- Peck, V. L., Yu, J., Kender, S., and Riesselman, C. R.: Shifting ocean carbonate chemistry during the Eocene-Oligocene climate transition: implications for deep-ocean Mg/Ca paleothermometry, *Paleoceanography*, 25, PA4219, doi:10.1029/2009PA001906, 2010.
- Persico, D. and Villa, G.: Eocene-Oligocene calcareous nannofossils from Maud Rise and Kerguelen Plateau (Antarctica): paleoecological and paleoceanographic implications, *Mar. Micropaleontol.*, 52, 153–179, 2004.
- Peterson, L. C. and Prell, W. L.: Carbonate dissolution in recent sediments of the eastern equatorial Indian Ocean: preservation patterns and carbonate loss above the lysocline, *Mar. Geol.*, 64, 259–290, 1985.
- Plancq, J., Grossi, V., Henderiks, J., Simon, L., and Mattioli, E.: Alkenone producers during late Oligocene–early Miocene revisited, *Paleoceanography*, 27, PA1202, doi:10.1029/2011PA002164, 2012.
- Premoli Silva, I. and Jenkins, D. G.: Decision on the Eocene-Oligocene boundary stratotype, *Episodes*, 16, 379–382, 1993.
- Raffi, I., Backman, J., Fornaciari, E., Pälike, H., Rio, D., Lourens, L., and Hilgen, F.: A review of calcareous nannofossil astrochronology encompassing the past 25 million years, *Quaternary Sci. Rev.*, 25, 3113–3137, 2006.
- Riesselman, C. R., Dunbar, R. B., Mucciarone, D. A., and Kita-sei, S. S.: High resolution stable isotope and carbonate variability during the early Oligocene climate transition: Walvis Ridge (ODP Site 1263), in: Antarctica: A Keystone in a Changing World-Online Proceedings of the 10th ISAES, edited by: Cooper, A. K., Raymond, C. R., and the 10th ISAES Editorial Team, *US Geol. Surv.*, doi:10.3133/of2007-1047.srp095, 2007.
- Rost, B., Riebesell, U., Burkhardt, S., and Sültemeyer, D.: Carbon acquisition of bloom-forming marine phytoplankton, *Limnol. Oceanogr.*, 48, 55–67, 2003.
- Rugenstein, M., Stocchi, P., von der Heijdt, A., Dijkstra, H., and Brinkhuis, H.: Emplacement of Antarctic ice sheet mass circum-polar ocean flow, *Global Planet. Change*, 118, 16–24, 2014.
- Saavedra-Pellitero, M., Flores, J. A., Baumann, K.-H., and Sierro, F. J.: Coccolith distribution patterns in surface sediments of Equatorial and Southeastern Pacific Ocean, *Geobios*, 43, 131–149, 2010.

- Salamy, K. A. and Zachos, J. C.: Latest Eocene-early Oligocene climate change and Southern Ocean fertility: inferences from sediment accumulation and stable isotope data, *Palaeogeogr. Palaeoclimatol.*, 145, 61–77, 1999.
- Sarnthein, M. and Winn, K.: Reconstruction of low and middle latitude export productivity, 30 000 years BP to present: implication for global carbon reservoir, in: *Climate-Ocean Interaction*, edited by: Schlesinger, M. E., Kluwer Academic Publishers, 319–342, 1990.
- Schumacher, S. and Lazarus, D.: Regional differences in pelagic productivity in the late Eocene to early Oligocene – a comparison of southern high latitudes and lower latitudes, *Palaeogeogr. Palaeoclimatol.*, 214, 243–263, 2004.
- Sijp, W. P., von der Heydt, A. S., Dijkstra, H. A., Flögel, S., Douglas, P. J., and Bijl, P. K.: The role of ocean gateways on cooling climate on long time scales, *Global Planet. Change*, 119, 1–22, 2014.
- Spencer-Cervato, C.: The Cenozoic deep sea microfossil record: explorations of the DSDP/ODP sample set using the Neptune Database, *Palaeontol. Electron.*, 2, 2, 270 pp., 1999.
- Thomas, E.: Late Cretaceous through Neogene deep-sea benthic foraminifers (Maud Rise, Weddell Sea, Antarctica), in: *Proceedings ODP, Scientific Results*, College Station, TX (Ocean Drilling Program), 113, 571–594, 1990.
- Thomas, E.: Middle Eocene – late Oligocene bathyal benthic foraminifera (Weddell Sea): faunal changes and implications for ocean circulation, in: *Late Eocene-Oligocene climatic and biotic evolution*, edited by: Prothero, D. R. and Berggren, W. A., Princeton University Press, 245–271, 1992.
- Thomas, E.: Cenozoic mass extinctions in the deep sea: what disturbs the largest habitat on Earth?, in: *Large ecosystem perturbations: causes and consequences*, edited by: Monechi, S., Cocconi, R., and Rampino, M., *Geol. S. Am. S.*, 424, 1–23, 2007.
- Thomas, E. and Gooday, A. J.: Cenozoic deep-sea benthic foraminifers: tracers for changes in oceanic productivity?, *Geology*, 24, 355–358, 1996.
- Tori, F.: Variabilità climatica e ciclicità nell'intervallo Eocene Oligocene: dati dai nannofossili calcarei, Ph.D. thesis, Department of Earth Sciences, University of Florence, Italy, 222 pp., 2008 (in Italian).
- Villa, G., FIORONI, C., Pea, L., Bohaty, S., and Persico, D.: Middle Eocene-late Oligocene climate variability: calcareous nannofossil response at Kerguelen Plateau, Site 748, *Mar. Micropaleontol.*, 69, 173–192, 2008.
- Villa, G., FIORONI, C., Persico, D., Roberts, A. P., and Florindo, F.: Middle Eocene to Late Oligocene Antarctic glaciation/deglaciation and Southern Ocean productivity, *Paleoceanography*, 29, 223–237, doi:10.1002/2013PA002518, 2014.
- Wade, B. S. and Pälike, H.: Oligocene climate dynamics, *Paleoceanography*, 19, PA4019, doi:10.1029/2004PA001042, 2004.
- Wade, B. S. and Pearson, P. N.: Planktonic foraminiferal turnover, diversity fluctuations and geochemical signals across the Eocene/Oligocene boundary in Tanzania, *Mar. Micropaleontol.*, 68, 244–255, 2008.
- Wei, W. and Wise, S. W.: Biogeographic gradients of middle Eocene–Oligocene calcareous nannoplankton in the South Atlantic Ocean, *Palaeogeogr. Palaeoclimatol.*, 79, 29–61, 1990.
- Winter, A., Jordan, R. W., and Roth, P. H.: Biogeography of living coccolithophores in ocean waters, in: *Coccolithophores*, edited by: Winter, A. and Siesser, W. G., 161–177, 1994.
- Young, J. R., Geisen, M., and Probert, I.: A review of selected aspects of coccolithophore biology with implications for paleodiversity estimation, *Micropaleontology*, 51, 267–288, doi:10.2113/gsmicropal.51.4.267, 2005.
- Young, J. R., Bown P. R., and Lees, J. A.: Nannotax3 website, International Nannoplankton Association, 21 April 2014, <http://ina.tmsoc.org/Nannotax3> (last access: 21 March 2015), 2014.
- Zachos, J. C. and Kump, L. R.: Carbon cycle feedbacks and the initiation of Antarctic glaciation in the earliest Oligocene, *Global Planet. Change*, 47, 51–66, 2005.
- Zachos, J. C., Quinn, T. M., and Salamy, K. A.: High-resolution (104 years) deep-sea foraminiferal stable isotope records of the Eocene-Oligocene climate transition, *Paleoceanography*, 11, 251–266, doi:10.1029/96PA00571, 1996.
- Zachos, J., Pagani, M., Sloan, L., Thomas, E., and Billups, K.: Trends, rhythms, and aberrations in global climate 65 Ma to present, *Science*, 292, 686–693, 2001.
- Zachos, J. C., Kroon, D., Blum, P., and Shipboard Scientific Party: Site 1263, in: *Proceedings ODP, Initial Reports*, College Station, TX (Ocean Drilling Program), 208, 1–87, 2004.
- Zhang, J., Wang, P., Li, Q., Cheng, X., Jin, H., and Zhang, S.: Western equatorial Pacific productivity and carbonate dissolution over the last 550 kyr: foraminiferal and nannofossil evidence from ODP Hole 807A, *Mar. Micropaleontol.*, 64, 121–140, 2007.
- Zhang, Y. G., Pagani, M., Liu, Z., Bohaty, S. M., and DeConto, R. M.: A 40-million-year history of atmospheric CO₂, *Philos. T. Roy. Soc. A.*, 371, 20130096, doi:10.1098/rsta.2013.0096, 2013.